Quaternary Research (2023), **116**, 30–45
doi:10.1017/qua.2023.37

Research Article

Middle to Late Holocene lake evolution and its links with westerlies and Asian monsoon in the middle part of the Hexi Corridor, NW China

Simin Peng[a], Yu Li[a], Xueru Zhou[a], Lu Hao[a], Hebin Liu[a], Zhansen Zhang[a] and Haiye Li[a]

[a]Key Laboratory of Western China's Environmental Systems (Ministry of Education), College of Earth and Environmental Sciences, Observation and Research Station on Eco-Environment of Frozen Ground in the Qilian Mountains, Lanzhou University, Lanzhou, 730000, China.

Abstract

The interpretation and understanding of the relationship between Middle to Late Holocene climate change in monsoon margins of northwest China with the westerlies and Asian monsoon (AM) remain controversial. Here we present a new multi-proxy sedimentary dataset from the Heihe River basin in the middle part of the Hexi Corridor on the northern margin of the Qinghai-Tibet Plateau (QTP), which is a sensitive zone for the interaction between the westerlies and AM. Fluctuations in grain size, $\delta^{13}C_{org}$, $\delta^{18}O$, magnetic susceptibility, total organic carbon, total nitrogen, and C/N ratio document regional lake and climate evolution since 5334 cal yr BP. Results show that climate conditions on the millennial timescale are humid in the late Middle Holocene (MH) and dry to wet in the Late Holocene (LH). Combined with the multi-model ensemble simulation from PMIP3-CMIP5, high lake levels and wetter climate in the late MH are closely linked to the strengthening Asian summer monsoon. Simultaneously, the slight wetting trend since the late LH may be the superimposing effect of enhanced westerlies and the weakening Asian winter monsoon. These findings can provide insights into the interpretation of the interaction between the westerlies and AM during the Holocene in East Asia.

Keywords: Lake evolution, Holocene, Westerlies, Asian monsoon, Hexi Corridor, Paleoclimate reconstruction and simulation, China

(Received 28 September 2022; accepted 19 June 2023)

INTRODUCTION

The effect of the relationship between the Asian monsoon (AM) and the mid-latitude westerlies on climate change in the Asian middle latitudes is an intricate yet crucial subject (Y. Wang et al., 2005; Chen et al., 2010, 2015; P. Wang et al., 2017; G. Li et al., 2022). Generally speaking, the AM and westerlies show different climate evolutionary patterns on long-term timescales as a result of alternative driving mechanisms (Nagashima et al., 2007; Chen et al., 2019). The monsoon climate pattern in East Asia manifesting as the humid Early Holocene (EH) and drier LH is out of phase with the typical westerlies-dominated climate in arid Central Asia, which is characterized by dry EH and wet LH (Chen et al., 2008; An et al., 2012; Wang and Feng, 2013; Li et al., 2021; Gao et al., 2023). Many studies in recent years suggested that the interaction between the westerlies and AM can be viewed as an explanation for the spatiotemporal difference in the precipitation pattern in the Asian middle latitudes (Nagashima et al., 2011; Chiang et al., 2015; Zhang et al., 2018; Li et al., 2020). On long-term timescales, the westerly jet path over East Asia is the main factor determining the location of the Asian summer monsoon rain belt (Sampe and Xie, 2010; Kong et al., 2017; Herzschuh et al., 2019). When earlier seasonal northward migration of the westerly jet axis occurs during the warm period, the Asian summer monsoon rainband shifts northward earlier, allowing more abundant precipitation in the northwestern margin of the Asian summer monsoon (Nagashima et al., 2013). At the same time, despite weakening of the summer monsoon, the larger ice sheet and lower North Atlantic sea surface temperature during the cold period led to an increase in the meridional temperature gradient and southward migration of the westerlies, bringing more water vapor to the northwestern margin of the Asian summer monsoon (Lan et al., 2021). Consequently, specific contributions and influencing mechanisms of the westerlies and AM to regional climate change remain controversial.

Climatic and environmental changes in the middle part of the Hexi Corridor, controlled by the westerlies and AM, are climatically sensitive and ideally located for paleoclimate research (Cheng et al., 2013; Wang et al., 2013; Chen et al., 2016a). In the past few decades, a number of attempts have been made to investigate a range of environmental and climatic reconstructions in the Hexi Corridor and its surroundings based on various paleoclimatic archives, such as lake sediments (Shen et al., 2005; Zhao et al., 2007; Chen et al., 2016a; Qiang et al., 2017), aeolian sediments (Lu et al., 2011; Liu et al., 2012; Sun et al., 2012; Li et al., 2020), ice cores (Thompson et al., 1988; Yao and Thompson, 1992), and tree rings (Gou et al., 2015; Yang et al., 2021). However, the debate continues about the climate evolutionary history due to nonuniform paleoclimate records from

Corresponding author: Yu Li; Email: liyu@lzu.edu.cn

Cite this article: Peng S, Li Y, Zhou X, Hao L, Liu H, Zhang Z, Li H (2023). Middle to Late Holocene lake evolution and its links with westerlies and Asian monsoon in the middle part of the Hexi Corridor, NW China. *Quaternary Research* **116**, 30–45. https://doi.org/10.1017/qua.2023.37

different positions (An et al., 2006; Wang et al., 2010). Based on the processes and mechanisms of modern climate, the Asian summer monsoon plays a crucial role in climate change and water vapor transport in the Hexi Corridor (Fig. 1) (Li et al., 2012). Therefore, whether the range of influence of the Asian summer monsoon has changed and how effective moisture transport by westerlies contributes to the middle part of the Hexi Corridor are vital issues in studying regional climate evolution in the northern margin of the QTP.

Situated in the marginal zone of the Asian summer monsoon vapor transport, the Heihe River basin is a key experimental field for clarifying the history of interaction between the westerlies and AM (Fig. 1). Consequently, the Beihaizi (BHZ) paleolake section from the Heihe River basin in the middle part of the Hexi Corridor enables exploration of past climate change and its driving forces in the northern margin of the QTP (Fig. 2). In paleoclimatology, geochemical proxies (TOC [total organic carbon], TN [total nitrogen], C/N [percent total nitrogen/percent organic carbon ratio], $\delta^{13}C_{org}$ [organic carbon isotopes], and $\delta^{18}O$ [carbonate oxygen isotopes]), magnetic susceptibility, and grain size are widely used to indicate changes in past temperature, moisture conditions, vegetation status, etc. In this paper, we expound on a general framework for reconstructing climate changes over the last 5334 years based on the analysis of multiple proxies in the BHZ sediments. In addition, paleoclimate models from the Paleoclimate Modeling Intercomparison Project 3 (PMIP3) were selected to visually investigate the relationship between climate and environment evolution with the westerlies and AM. A better understanding of the interaction between different atmospheric circulation systems will be of great significance for characterizing future variability of the hydroclimate in climate-sensitive areas during increased global warming.

REGIONAL SETTING

The BHZ section (40°13′N, 98°45′E), located in Xiba town, Jinta County, Gansu Province in northwestern China, was generated from the Beihaizi paleolake in the Jinta Basin in the middle part of the Hexi Corridor (Fig. 2a). The Jinta Basin is the terminal area of the Beidahe River (Taolai River), which originates from the Qilian Mountains in the northern QTP and flows through the alluvial plain in the middle reaches of the Heihe River (Zhang et al., 2011). The Jinta Basin is surrounded by the Beishan Mountains and Jinta Nanshan in the north and south, respectively, and is connected to the Huahai Basin in the west and the Badain Jaran Desert in the east (Fig. 2). The terrain of the basin is higher in the south and lower in the north, and gradually inclines from the southwest to the northeast. Many studies have established that Quaternary fluvial and lacustrine sediments were deposited in the paleolake basin in the northern Jinta Basin (Dodson et al., 2009; X. Li et al., 2010, 2011, 2013; Wang et al., 2011; Feng et al., 2020). At present, the Beihaizi paleolake has completely dried up, and Beihaizi wetland park was built at the northern margin of the alluvial fan of the Beidahe River. Most of the lacustrine plains in the paleolake basin are occupied by *Tamarix* and have developed gypsiferous gray-brown desert soil, meadow soil, and swamp soil (Li, 1998; Wang et al., 2011). As an arid area in northwest China, the study area has a typical continental climate with average annual temperature of 8°C, average annual precipitation of 54.4–77.7 mm, and potential evaporation of 3000 mm/year. Desert vegetation, including *Tamarix chinensis*, *Agriophyllum squarrosum*, *Apocynum venetum*, and *Achnatherum splendens*, is widely distributed in the study area (Zhang et al., 2020). According to an analysis of modern climatology, the Asian summer monsoon rarely reaches the sampling site compared to the westerlies (Fig. 1). As a result of the climate complexity in the monsoon marginal zone, the sensitive location enables sediment proxies of the BHZ section to record the interaction between the westerlies and AM.

MATERIALS AND METHODS

Sample collection

The BHZ sedimentary samples were collected from bottom to top with a sampling interval of 12.5 cm for 527–252 cm and 2 cm for 252–16 cm, respectively (Fig. S1; Table S2). Since the uppermost 16 cm of the BHZ section is modern soil, no sampling was performed. Ultimately, the BHZ section (section depth = 527 cm, sampling depth = 511 cm) yielded 140 sedimentary samples.

AMS^{14}C dating

Terrestrial plant residue is usually viewed as one of the most reliable materials for ^{14}C dating (Zhang et al., 2006). However, considering the lack of available terrestrial plant residue for dating, organic matter obtained from the bulk sediments is often used for ^{14}C dating (Sun et al., 2009; Wen et al., 2010; An et al., 2011). Consequently, the bulk organic matter of 58 samples in the BHZ section was selected for Accelerator Mass Spectrometry Radiocarbon Dating (AMS^{14}C) (Table S1). The OxCal v4.4.2 program (Bronk Ramsey, 2009; Bronk Ramsey and Lee, 2013) and IntCal20 atmospheric curve (Reimer et al., 2020) provided calibration of radiocarbon ^{14}C dates (0 BP = AD 1950). The AMS^{14}C ages of the BHZ section were all measured in the Laboratory of Scientific Archaeology and Preservation of Cultural Relics, School of Archaeology and Museology, Peking University, China.

Proxies used

Organic carbon isotopes ($\delta^{13}C_{org}$), carbonate oxygen isotopes ($\delta^{18}O$), grain size (GS), total organic carbon (TOC), total nitrogen (TN), the percent total nitrogen/percent organic carbon (C/N) ratio, and magnetic susceptibility (MS) of the BHZ section were measured (Table S2). Eighty-one lake sediment samples were used for $\delta^{13}C_{org}$, $\delta^{18}O$, TOC, and TN testing. $\delta^{13}C_{org}$ (‰) and $\delta^{18}O$ (‰) values were measured, respectively, by the MAT253plus+FlashEA and MAT253plus+GasBench in the Beijing Createch Testing Technology Co. Ltd, Beijing, China. TOC (%) and TN (%) were measured by Vario-III elemental analyzer with an analytical error of <0.1% in the Analysis and Testing Center of Lanzhou University, Lanzhou, China. MS and GS analyses of 140 lake sediment samples were completed in the Key Laboratory of Western China's Environmental Systems (Ministry of Education), Lanzhou, China. MS was determined using the Bartington MS2 logger. In this study, frequency magnetic susceptibility percentages (χ_{fd} %) were used as MS parameter to indicate climate changes (Ji and Xia, 2007). Grain-size distribution was measured using a Malvern Mastersizer 2000 particle analyzer, which has a measurement range of 0.02–2000 μm and a repeated error of <3%. Subsequently, we calculated three grain-size parameters, including mean GS (%), median GS (%), and modal GS (%). In addition, the division of sedimentary facies

https://doi.org/10.1017/qua.2023.37 Published online by Cambridge University Press

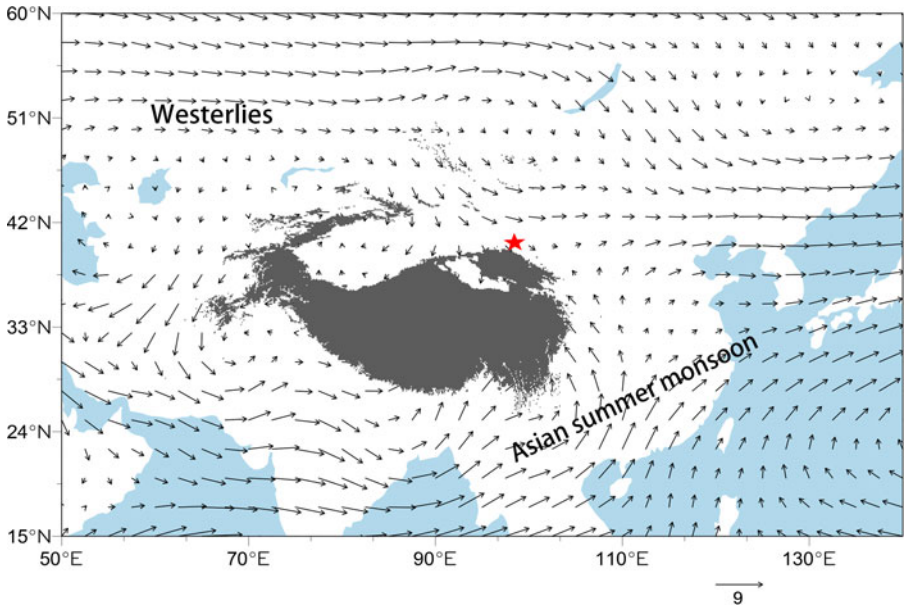

Figure 1. Circulation conditions and location of the study area (red star). The arrows represent the monthly mean 850 hPa (hectoPascals) wind field (m/s) in summer (JJA, June–July–August) during 1969–2018 (data from the NCEP/NCAR Global Reanalysis 1 dataset; Kalnay et al., 1996).

based on grain size, such as clay (<4 μm), silt (4–63 μm), and sand (>63 μm) can provide a good understanding of the sedimentary environment (Terry and Goff, 2014). Nevertheless, grain-size data are still problematic because of the difficulty in differentiating sediment-transport mechanisms merely by sedimentary facies and grain size in finely laminated lacustrine deposits (X. Liu et al., 2016). Therefore, we also used the end-member modeling (EMM) method to more rationally decompose the GS distribution data into sensitive grain-size components of terrestrial, fluvial, and aeolian sediments, and to obtain valuable information on geological processes and paleoenvironments (Kranck et al., 1996; Prins et al., 2002; Weltje and Prins, 2003; Meyer et al., 2013; Dietze et al., 2014; Greig and David, 2015).

Paleoclimate simulations

The equilibrium "time-slice" simulations for 6000 cal yr BP (MH) and pre-industrial (PI) from the $PMIP_3$- (Palaeoclimate Modelling Intercomparison Project Phase 3) CMIP5 (Coupled Model Intercomparison Project Phase 5) were synthesized to understand the role of the atmosphere circulation system and analyze the dynamic mechanism of climate conditions in the BHZ section during the MH and LH. We applied a multi-model ensemble simulation from 11 models: BCC-CSM1-1 (Beijing Climate Center Climate System Model), CNRM-CM5 (Centre National de Recherches Météorologiques-Climate Model Version 5), CCSM4 (Community Climate System Model Version 4), CSIRO-Mk3-6-0 (Commonwealth Scientific and Industrial Research Organisation), GISS-E2-R (Goddard Institute for Space Studies), MIROC-ESM (Model for Interdisciplinary Research on Climate-Earth System Model), FGOALS-s2 (Flexible Global Ocean-Atmosphere-Land system model, Spectral Version 2), FGOALS-g2 (Flexible Global Ocean-Atmosphere-Land system model, Grid-point Version 2), IPSL-CM5A-LR (Institut Pierre Simon Laplace-Climate Model 5A-Low Resolution), MPI-ESM-P (Max Planck Institute Earth System Model-Paleoclimate), and MRI-CGCM3 (Meteorological Research Institute Coupled Global Climate Model Version 3). The variables used are precipitation, evaporation, meridional winds, and zonal wind, which are available at https://esgf-node.llnl.gov/search/esgf-llnl/. The name, affiliation, country, resolution, and references of the models are shown in Table 1. In view of the different horizontal resolution of the output data, we used the bilinear interpolation method to interpolate the output data of all models to a resolution of 1° × 1° to facilitate model aggregation.

RESULTS

Lithological description

Based on observations of sediment color and texture (Figs. S1, 3), the lithology characteristics from top to bottom can be approximately divided into eight parts: (1) 16–125 cm, light brown silt, large parts of which could be covered by wind-blown loess or aeolian sand; (2) 125–180 cm, light brown clay; (3) 180–230 cm, dark green clay; (4) 230–240 cm, light gray sand; (5) 240–300 cm, dark green silty clay; (6) 300–400 cm, gray clayey silt; (7) 400–460 cm, gray silty clay; (8) 460–540 cm, gray-black silty clay with humic mud.

Chronology

In arid and semi-arid regions, the reservoir effect may cause AMS ^{14}C dating results of bulk organic matter in lacustrine sediments to be older than the real ages (Liu et al., 2009; Long et al., 2011). However, more-reliable dating materials, such as plant residues or charcoal, cannot be found in the BHZ section, resulting in the inability to obtain an accurate age of the reservoir effect. Additionally, due to the lack of detailed investigation on the embankment of Beihaizi paleolake, it is impossible to quantify the age of drying of the Beihaizi paleolake. Therefore, surface sediments of the Beihaizi paleolake cannot be used to determine the modern reservoir age of the paleolake. Hence, we set the reservoir age as 2000 yr and preliminarily removed the reservoir effect from samples below ~125 cm, mainly in light of the median value of existing reservoir ages, which, in adjacent regions, is ca. 2500 yr in Huahai paleolake (Wang et al., 2013), ca. 2000 yr in eastern

https://doi.org/10.1017/qua.2023.37 Published online by Cambridge University Press

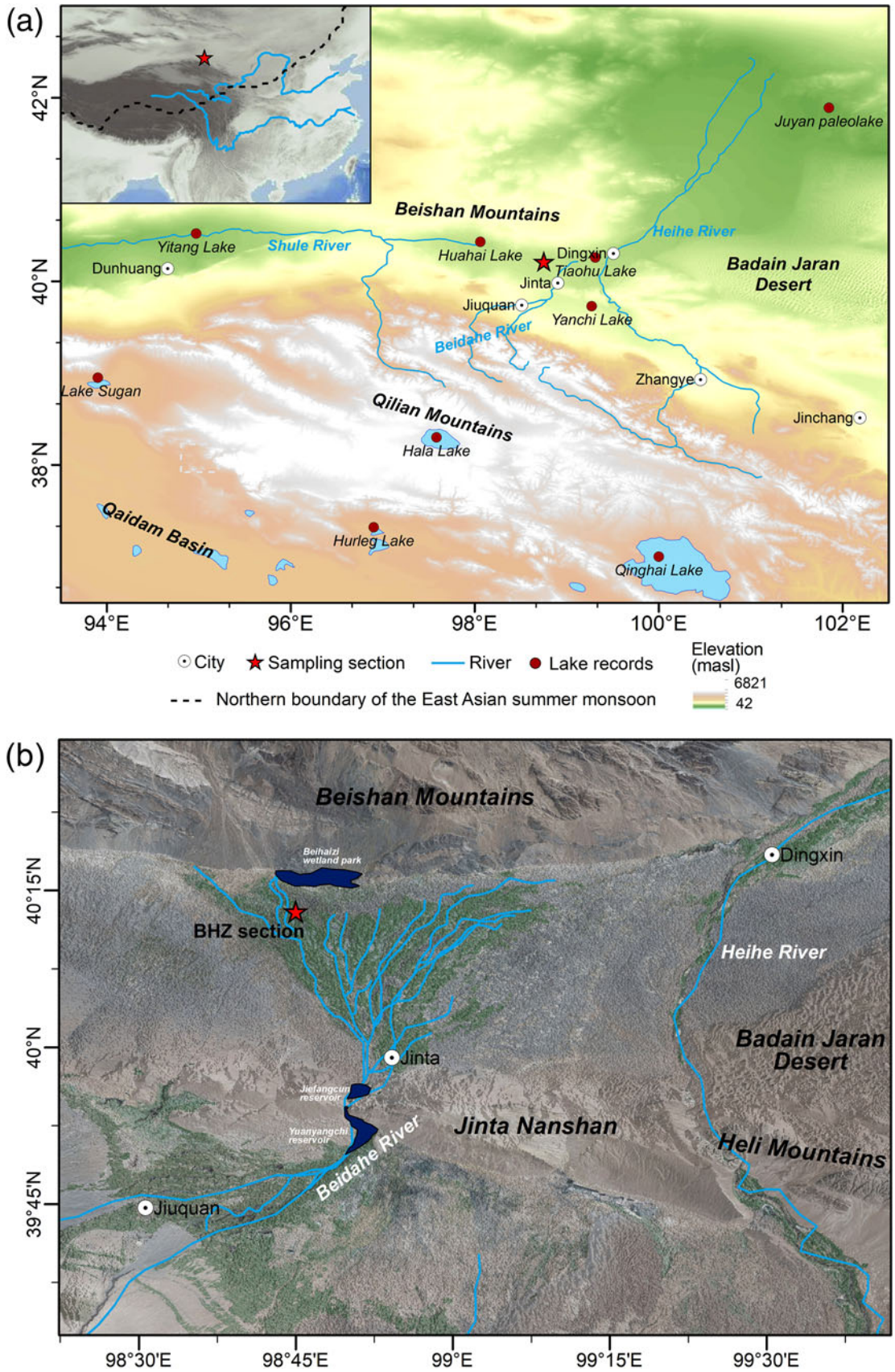

Figure 2. (**a**) Locations and distribution of the BHZ section (red star) and other lake records (red dots) in the adjacent area. The climatological northern boundary of the East Asian summer monsoon (black dashed line) during 1965–2014 is from Wang et al. (2012). (**b**) Satellite image showing the Jinta Basin, the water system of the Beidahe River, and key geographic features mentioned in the text. The Beidahe River used to flow into the Heihe River in the town of Dingxin, northeast of the Jinta Basin. However, after the completion of the Yuanyangchi Reservoir and the Jiefangcun Reservoir in the 1970s, the amount of downstream water dropped sharply, making it impossible for the Beidahe River to reach Dingxin.

https://doi.org/10.1017/qua.2023.37 Published online by Cambridge University Press

Table 1. Basic information about climate models from PMIP3-CMIP5 used in this study.

Model	Affiliation and country	Resolution (°)	Variables*	References
BCC-CSM1-1	BCC, China	128 × 64	pr, evp	Randall et al. (2007)
CNRM-CM5	CNRM-CERFACS, France	256 × 128	pr, evp, ua, va	Voldoire et al. (2013)
CCSM4	NCAR, USA	288 × 192	pr, evp, ua, va	Gent et al. (2011)
CSIRO-Mk3-6-0	CSIRO-QCCCE, Australia	192 × 96	pr, evp	Rotstayn et al. (2010)
GISS-E2-R	NASA GISS, USA	144 × 89	pr, evp, ua, va	Schmidt et al. (2014)
MIROC-ESM	MIROC, Japan	128 × 64	pr, evp, ua, va	Watanabe et al. (2011)
FGOALS-s2	IAP, China	128 × 108	pr, evp	Briegleb et al. (2004)
FGOALS-g2	IAP, China	128 × 60	pr, evp, ua, va	L. Li et al. (2013)
IPSL-CM5A-LR	IPSL, France	96 × 96	pr, evp, ua, va	Dufresne et al. (2013)
MPI-ESM-P	MPI-M, Germany	192 × 96	pr, evp, ua, va	Raddatz et al. (2007)
MRI-CGCM3	MRI, Japan	320 × 160	pr, evp, ua, va	Yukimoto et al. (2012)

*pr = precipitation; evp = evaporation; ua = zonal wind; va = meridional wind

Juyan paleolake (Hartmann and Wünnemann, 2009), and ca. 1080 yr in lakes of the Badain Jaran Desert (Hofmann and Geyh, 1998; Yang et al., 2010). After removing the reservoir effect, the AMS ^{14}C ages were calibrated (0 BP = AD 1950) using the OxCal v4.4.2 program and IntCal20 atmospheric curve (Table S1).

Figure 3 shows the distributions of calibrated ^{14}C ages and the stratigraphic characteristics of the BHZ section. Based on the integrated analysis of the chronology, we determined that the age can be divided into three parts: the upper, middle, and bottom layers. The ages of the upper layer are in the LH, the ages of the middle layer are disordered, and the ages of the bottom layer basically belong to the MH except for the two abnormally old ages. Meanwhile, the slight fluctuations of TOC and mean GS in the upper and bottom layers indicate relatively stable deposition conditions, which suggests that the dates of these two layers are reliable and are likely less contaminated. However, the TOC and mean GS in the middle layer vary greatly, which is related to the reworking effect, the input of "old carbon," and deposition instability (Sun et al., 2010). To this end, we first eliminated the abnormally old ages at 402–389.5 cm, 352–238 cm, and 182–150 cm in the middle layer (Table S1). The abnormally young age at 230 cm was also discarded because of its irregularity in the overall distribution of the chronology results and its distinct inconsistency with establishment of the Holocene age.

In this study, the traditional mathematical fitting method is used to establish the age-depth model (X. Liu et al., 2016; Li et al., 2020). The logarithmic curve was finalized as the age-depth model of 32 dates due to having the highest correlation after eliminating anomalous ages ($y = 1200.2 \bullet \ln(x) - 2187.3$) (Y. Zhao et al., 2007; C. Zhao et al., 2010; Wu et al., 2020) (Fig. 3), which provides a continuous sedimentary record since 5334 cal yr BP. The chronology conducted by calibrated age-depth model covers ca. 1281–5334 cal yr BP.

Sedimentary environment based on GS and MS

We analyzed the variations of six grain-size proxies with depth (Fig. 4a). The average median GS, mean GS, modal GS, clay, silt, and sand are 56.03 μm, 37.69 μm, 74.93 μm, 21.48%, 52.09%, and 26.43%, respectively. The GS distributions in the BHZ section are mainly composed of silt fractions, with contribution percentages of 14.68–81.81%. The overall variations of four grain-size proxies (median GS, mean GS, modal GS, and sand) exhibit generally similar trends, which is in contrast to two finer-grained fractions (clay and silt). In addition, there is an obvious shift in six grain-size proxies at ~230 cm and ~125 cm. The MS in the BHZ sediments exhibits significant fluctuations (Fig. 4a). The silt- and clay-dominated sediments at 230–125 cm have a high MS value as a whole, which indicates that high MS corresponds to the finer GS with magnetic minerals.

As shown in Figure 4b, EMM analysis in the BHZ section yields an optimal model with four EMs characterized by a single peak mode. The peak of EM1 at 1–10 μm indicates deep lacustrine deposits with fine grain size. In contrast, EM4 has a narrow peak at 100–400 μm, exhibiting stronger transport capacity and a high-energy deposition environment. Both EM2 and EM3 have a broad mode in the silt component, characterized by peaks of 10–30 μm in the fine-grain part and of 50–100 μm in the coarse-grain part, respectively. The endmember sequences generated by the abundance variations of all sediment samples at four EMs are shown in Figure 4c. The boundary of sedimentary facies at ~230 cm and ~125 cm is still very obvious, which is consistent with the variation in the six grain-size proxies (Fig. 4a). The variation in coarse grain size, which is dominant in EM4, has a similar trend to the mean GS, median GS, mode GS, and sand content. The deep lacustrine endmember EM1 primarily highlights the lake-dominated sedimentary environment at ~230–125 cm and 527–400 cm.

Combined GS proxies, MS, and EMM analysis show that the sedimentary environments of the BHZ section can be divided into four intervals: (1) aeolian deposits (16–125 cm) with an increasing trend of coarse-grained composition and decreasing trend of clay and silt, among which the sand content slightly decreased and the silt content slightly increased in fluctuation at 16–75 cm; (2) increased clay and silt and decreased coarse-grained composition (125–230 cm), belonging to lacustrine deposits and containing organic matter and carbon; (3) lakeside deposits with dominant sand content (230–240 cm); and (4) relatively small-amplitude variations (240–527 cm) with slightly increased coarse-grained composition and decreased fine-grained

https://doi.org/10.1017/qua.2023.37 Published online by Cambridge University Press

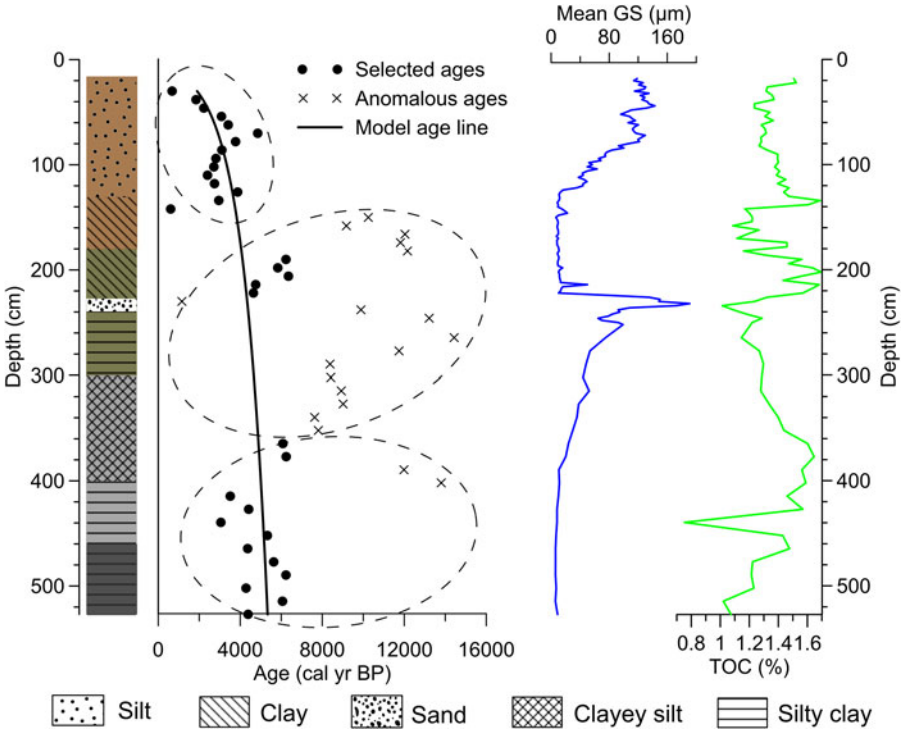

Figure 3. Age-depth model, lithology, and variation of mean GS and TOC with depth of the BHZ section.

composition and clay, from deep lacustrine at 400–527 cm to shallow lacustrine deposit at 240–400 cm.

Geochemical and isotopic results

The average values of TOC, TN, C/N, $\delta^{13}C_{org}$, and $\delta^{18}O$ in the BHZ sediments are 1.35%, 0.04%, 36.29%, −23.6‰, and −9.33‰, respectively (Fig. 5). The C/N ratio is 16.80–80.67% and is mostly >20%, indicating that the organic matter in the BHZ section was mainly contributed by terrestrial organisms. Meanwhile, the range of $\delta^{13}C_{org}$ is between −25‰ and −22‰, most of which is within the $\delta^{13}C_{org}$ distribution range of C_3 plants (Farquhar et al., 1989; Bowen, 1991). As a result, it can be accurately determined, through the composition of the C/N and $\delta^{13}C_{org}$, that the organic matter in the BHZ section mainly comes from C_3 land plants (Fig. 5c). By analyzing the scatter correlation diagrams of TOC, C/N, and $\delta^{13}C_{org}$, the higher TOC values are accompanied by the higher C/N values and the negative $\delta^{13}C_{org}$ values (Fig. 5a, b). Figure 5d shows that all the proxies shift significantly at ~230 cm and are characterized by high TOC, TN, and C/N values, negative $\delta^{13}C_{org}$ values, and positive $\delta^{18}O$ values at 230–125 cm. At the same time, TOC, TN, and negative bias of $\delta^{13}C_{org}$ show a slightly increasing trend above ~75 cm.

DISCUSSION

Proxy Premises

The GS distribution of lake sediments can provide direct information on the lake level, hydrodynamic conditions, and sedimentary environment (Chen et al., 1999; Peng et al., 2005; Xiao et al., 2013). Generally, coarse GS indicates a dry climate in which the lake is shrinking and shallower in arid and semi-arid regions on long-term timescales (C. Liu et al., 2016; X. Liu et al., 2016; Hu et al., 2017; Wu et al., 2020).

The MS in lake sediments documents the sizes and types of magnetic minerals (Wu, 1993). Recently, comprehensive analyses of surface sediments in the Qilian Mountains confirmed that high MS values are usually enriched in fine-grained fractions and are positively correlated with regional precipitation (Y. Li et al., 2022; Peng et al., 2022). Some paleoclimate studies also claimed that high MS values are positively related to silt and clay content and indicate a humid environment (Zhang et al., 1998; Zhao et al., 2005).

The TOC in lake sediments, usually an indicator of vegetation coverage and primary productivity in watersheds and lakes, is widely applied to paleoclimate research (Aravena et al., 1992; Zhong et al., 2010). In arid and semi-arid regions, moisture conditions are the main limiting factors for plant growth, therefore, a humid climate usually corresponds to higher values of TOC (Y. Li et al., 2011).

C/N values reflect the ratio of aquatic to terrestrial organic matter and can be used to determine the source of organic matter in lake sediments (Meyers and Lallier-Vergès, 1999). During intervals of low lake levels, exposed lakeshore shoal zones are beneficial to terrestrial plant growth, thus increasing the contribution of terrigenous organic matter in lake sediments, which will lead to higher C/N ratios (Wu et al., 2015).

Organic matter $\delta^{13}C_{org}$ in lake sediments is mainly derived from terrestrial plants and aquatic plants, which can be identified by composition of the $\delta^{13}C_{org}$ and C/N. Meanwhile, photosynthetic types of C_3-like and C_4-like carbon fixation also exist in aquatic plants (Liu et al., 2013). Relevant reports of modern plants and surface sediments pointed out that climate elements (i.e., temperature and precipitation) are dominant factors controlling C_3/C_4 relative abundance in arid and semi-arid regions (Rao et al., 2012, 2017; Zhao et al., 2017; Y. Li et al., 2020, 2022).

https://doi.org/10.1017/qua.2023.37 Published online by Cambridge University Press

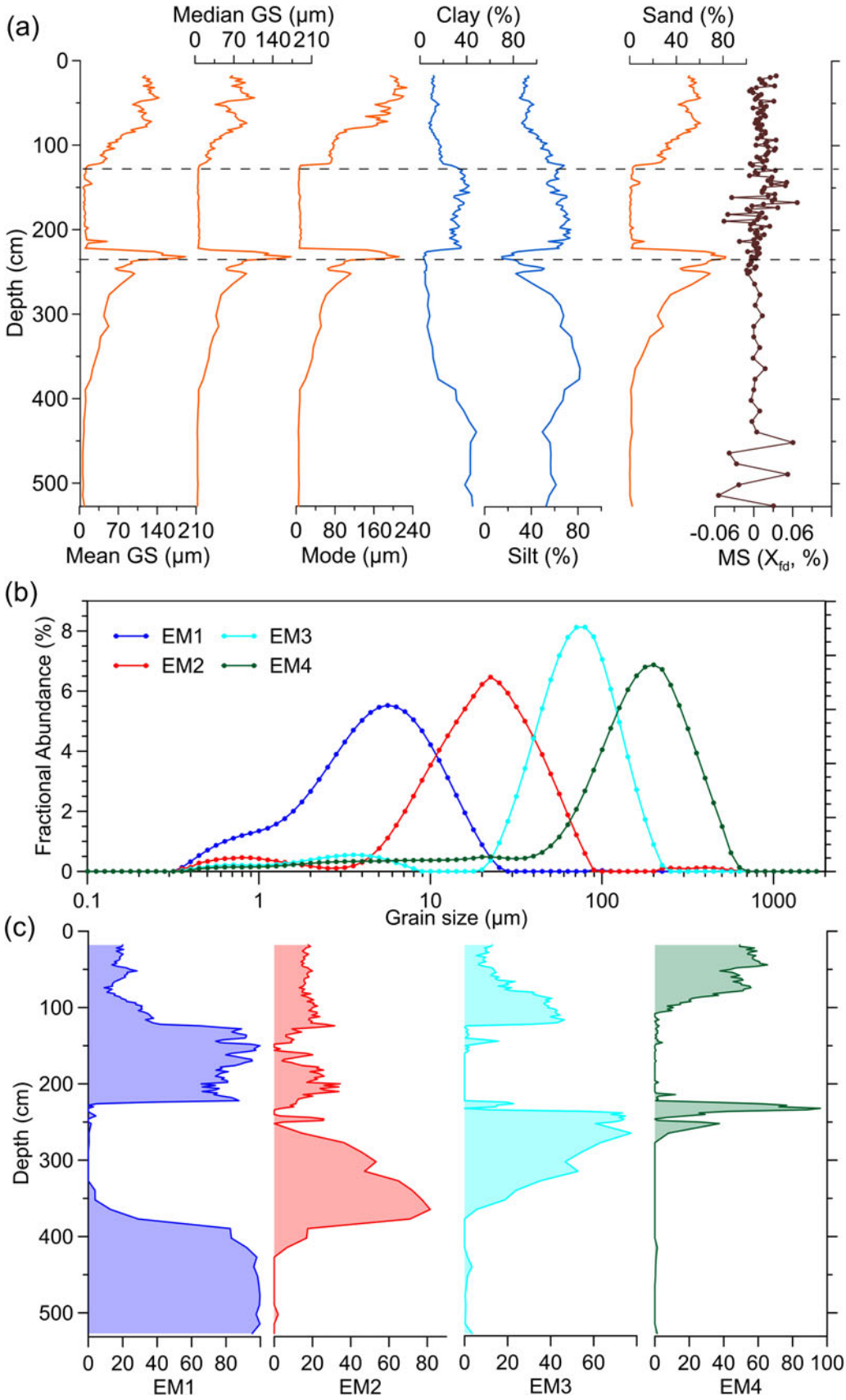

Figure 4. Results of GS and MS analyses. (**a**) Variations in mean GS, median GS, mode GS, clay, silt, sand, and MS from the BHZ section. Dashed lines indicate obvious grain-size shifts. (**b, c**) EMM results of the BHZ sediments: (**b**) grain-size distributions of four EMs; (**c**) abundance variations (%) of four EMs in a synthetic data set of the BHZ sediments.

https://doi.org/10.1017/qua.2023.37 Published online by Cambridge University Press

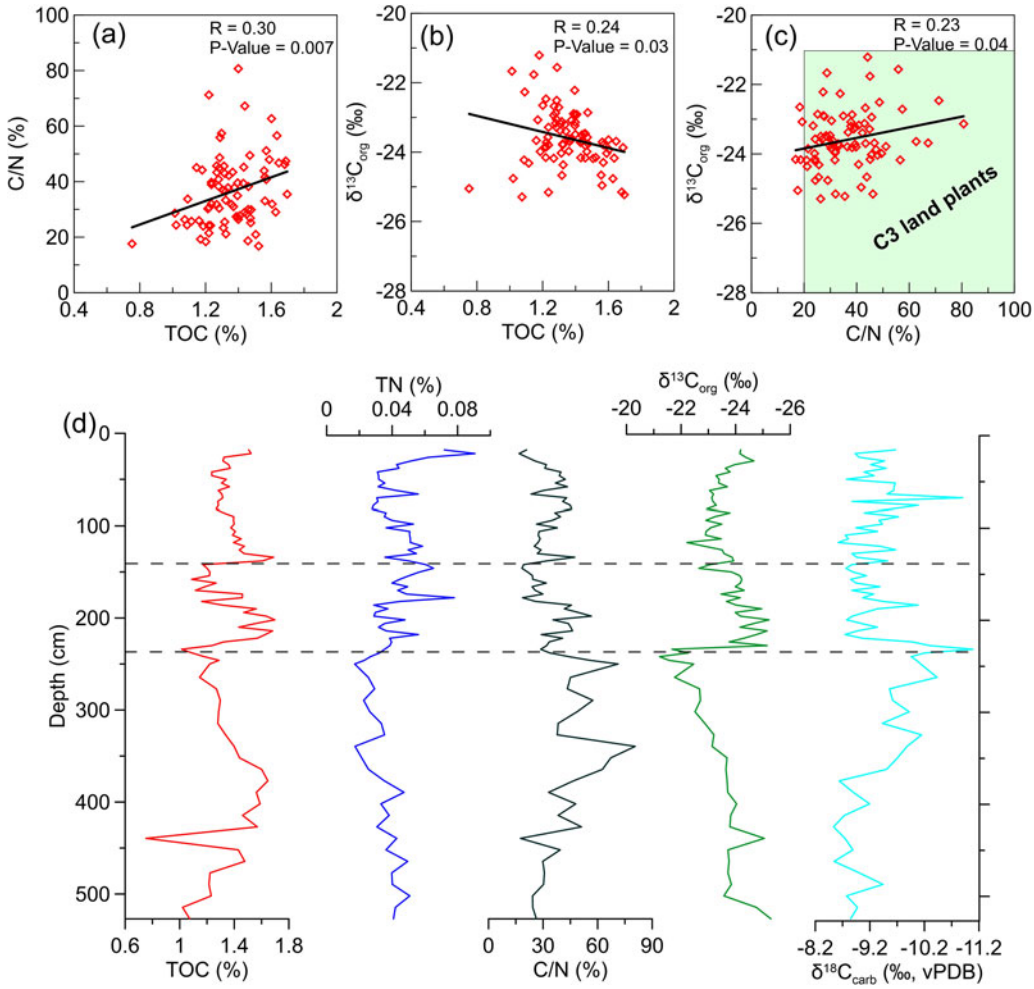

Figure 5. (**a–c**) Linear regressions (**a**) between TOC and C/N, (**b**) TOC and $\delta^{13}C_{org}$, and (**c**) $\delta^{13}C_{org}$ and C/N; R and P-values represent the value of each linear regression and the level of significance, respectively. (**d**) Variations in TOC, TN, C/N, $\delta^{13}C_{org}$, and $\delta^{18}O_{carb}$ with depth.

The carbonate $\delta^{18}O$ in lake sediments is mainly controlled by the $\delta^{18}O$ composition of lake water during carbonate precipitation. In closed lakes of arid and semi-arid regions, the lake water $\delta^{18}O$ is primarily affected by the precipitation/evaporation (P/E) or inflow/evaporation (I/E) ratios, so $\delta^{18}O$ records in lacustrine carbonate sediments can provide references to past hydrological and dry/wet changes (Lister et al., 1991; Qiang et al., 2005; Yu et al., 2009).

Evidence of lake and climate evolution in the BHZ section

The results of all proxies in the BHZ section show that there is a clear transition at ~230 cm, which is represented by a decrease in sand content (Fig. 4a) and an increase in organic matter (Fig. 5d) and is in line with the characteristics of lacustrine deposits (Berner, 1981). Combined with the age-depth model (Fig. 3), it is apparent that the age at 230–125 cm is approximately late MH (ca. 4400 to ca. 3500 cal yr BP). The change with depth of all climate proxies from the BHZ section is shown in Figure 6, reconstructing lake evolution since 5334 cal yr BP. TOC, C/N, MS, $\delta^{18}O$, and clay fluctuate sharply in the late MH. At about 4400–3500 cal yr BP, compared with overlying horizons, the BHZ section has negative $\delta^{13}C_{org}$, positive $\delta^{18}O$, and high clay, TOC, C/N, and MS. Meanwhile, TOC, MS, and negative bias of $\delta^{13}C_{org}$ and $\delta^{18}O$ show a slightly increasing trend since the late LH.

Based on our climatic/environmental interpretations of paleoclimate proxies, we can reconstruct climate evolutionary history since 5334 cal yr BP. During ca. 4400 to ca. 3500 cal yr BP, the clay and silt content in the BHZ section increased while the sand content decreased and the median GS is small (Fig. 6e), indicating weak hydrodynamics under high lake levels and humid environments in the late MH. Meanwhile, high MS values in the late MH confirm the development of fine grain size and more magnetic minerals under humid climate conditions in the BHZ section (Fig. 6f). Under humid climate conditions, the high lake level resulted in weak hydrodynamics, which is conducive to the development of fine grain size and more magnetic minerals (Hu et al., 2017). TOC values are relatively high in the late MH, suggesting higher primary productivity within the lake basin in the context of a humid climate (Fig. 6b, d). Compared to 5334 to ca. 4400 cal yr BP, low C/N values in the late MH may indicate that a rising lake level was beneficial to the growth of aquatic organisms, thereby increasing the proportion of aquatic plants in the organic matter of lake sediments (Fig. 6c) (Lan et al., 2013; Wu et al., 2015). Sedimentary $\delta^{13}C_{org}$ data in the BHZ section are mostly within the range of C_3 plants (Fig. 6b). Many previous studies showed that the $\delta^{13}C_{org}$ value of terrestrial C_3 plants

https://doi.org/10.1017/qua.2023.37 Published online by Cambridge University Press

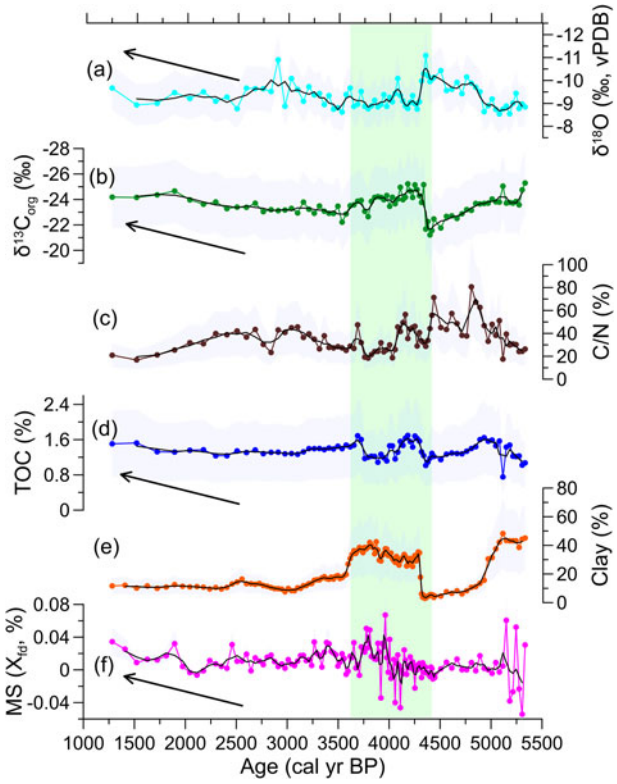

Figure 6. (**a–f**) Comparison of climate proxies ($\delta^{18}O$, $\delta^{13}C_{org}$, C/N, TOC, Clay, MS) from the BHZ section. The black lines and purple shading indicate the running average and error bar of climate proxies, respectively. Green shading represents the remarkably humid condition; arrows indicate wetting trends in the LH.

is driven by effective moisture and is more significantly correlated with precipitation than with temperature (Zheng and Shangguan, 2007; Kohn, 2010; Zhou et al., 2013). Our previous results of surface sediments in the Qilian Mountains demonstrated that the $\delta^{13}C_{org}$ of C_3 plants is more negative with increasing precipitation (Li et al., 2020). In addition, the $\delta^{13}C_{org}$ values of C_3-like plants, such as *Cladophora*, in lake sediments become more negative with increasing water depth (Liu et al., 2013). Thus, we suggest that negative $\delta^{13}C_{org}$ values indicate a relatively humid climate in Beihaizi paleolake, specifically manifesting as increased aquatic C_3 plants with high lake levels in the late MH and increase of terrestrial C_3 plants caused by increase in effective moisture since the late LH (Fig. 6b). Given the positive relationship between $\delta^{18}O$ and evaporation intensity (Horton et al., 2016), the positive $\delta^{18}O$ in the MH reflects enhanced evaporation by increased insolation and high air temperature (Kaufman et al., 2020) (Fig. 6a), which raises atmospheric humidity to enhance regional precipitation. Ultimately, high regional precipitation, indicated by GS, MS, and geochemical proxies, may have offset evaporative losses from the lake surfaces, resulting in a climate and environment with higher effective humidity (high P/E or I/E ratio) in the late MH (Herzschuh et al., 2014). With the temperature decline since the MH, the $\delta^{18}O$ depletion in the late LH probably mirrors a positive moisture balance (i.e., a high P/E or I/E ratio as the result of weakened evaporation) (Qiang et al., 2017).

The synthesis of all paleoclimate proxies confirms a humid late MH in the BHZ section. At the same time, although the grain size of lake sediments has not become significantly finer since the late LH, TOC, MS, $\delta^{13}C_{org}$, and $\delta^{18}O$ proxies indicate that the surrounding vegetation environment improved and the organic matter content in the sediments increased. We argue that despite the overall transition from a lacustrine sedimentary environment in the MH to an aeolian sedimentary environment in the LH, there is still a slight wetting trend during the late LH in the BHZ section.

Paleoclimate ensemble simulation of precipitation, evaporation, and corresponding effective moisture can give more intuitive evidence. Precipitation and evaporation during the MH are higher than during the PI in the BHZ section, and the magnitude of precipitation is greater (Fig. 7a, b). This further corroborates the results of proxy reconstruction (i.e., high evaporation represented by $\delta^{18}O$ depletion and high precipitation indicated by GS, MS, and geochemical proxies in the BHZ section). To clarify the moisture difference, we calculated the effective moisture represented by precipitation minus evaporation (P−E) (Fig. 7c). The result indicates that effective moisture during the MH in the BHZ section was higher than during the PI, which corresponds to the high P/E or I/E ratio.

Possible causes of regional climate evolution

Changes in atmospheric circulation patterns are important factors in affecting regional climate evolution and hydrological conditions. The climate and environmental records from the east part of the Hexi Corridor generally show monsoonal characteristics: a humid climate in the EH and MH, and gradually drying climate in the LH (Liu et al., 2007; Qiang et al., 2013). However, the middle part of the Hexi Corridor, located in the monsoon-westerly transition zone, presents a complex Holocene climatic change pattern that is not the same as either the monsoon-affected region or the westerlies-affected region (Zhao et al., 2007; Yan and Wünnemann, 2014; Li et al., 2020). Based on the paleoclimate ensemble simulation, we analyzed the climate regime anomalies between MH and PI to visually investigate the relationship between climate evolution in the BHZ section from the middle part of the Hexi Corridor and westerlies/AM. The southerly wind in the averaged and differential field at 850 hPa (hectoPascals) means that the Asian summer monsoon in the MH is more intense than that in the PI (Fig. 8a, b), which is consistent with the reconstruction of the East Asian summer monsoon from speleothem $\delta^{18}O$ records in south China (Yuan et al., 2004; Wang et al., 2001). Meanwhile, the increase in summer precipitation also indicates the remarkable contribution of intensified Asian summer monsoon to local precipitation in the BHZ section, further causing the MH humid climate (Fig. 8b). In comparison to the averaged wind fields at 200 hPa (Fig. 8c), the same wind direction and increasing winter precipitation in the winter differential field indicate that the westerlies strengthened in the winter during the PI compared to the MH (Fig. 8d). In addition, the differential wind field of the Asian winter monsoon between the PI and MH, unlike the averaged wind field, indicates a weaker Asian winter monsoon during the PI (Fig. 8e, f). In the LH, weakening of the Asian winter monsoon and then the increase in the winter water vapor supplement (Zhang et al., 2022), caused by the increase in winter insolation (Berger and Loutre, 1991), favored the improvement of vegetation growth and the preservation of organic matter (Xiao et al. 2002; Peng et al., 2022). Moreover, the increased insolation gradient was conducive to the gradual strengthening of westerlies in the LH, thereby increasing moisture transport to the BHZ section and the middle part of the Hexi Corridor (Jin et al., 2012;

https://doi.org/10.1017/qua.2023.37 Published online by Cambridge University Press

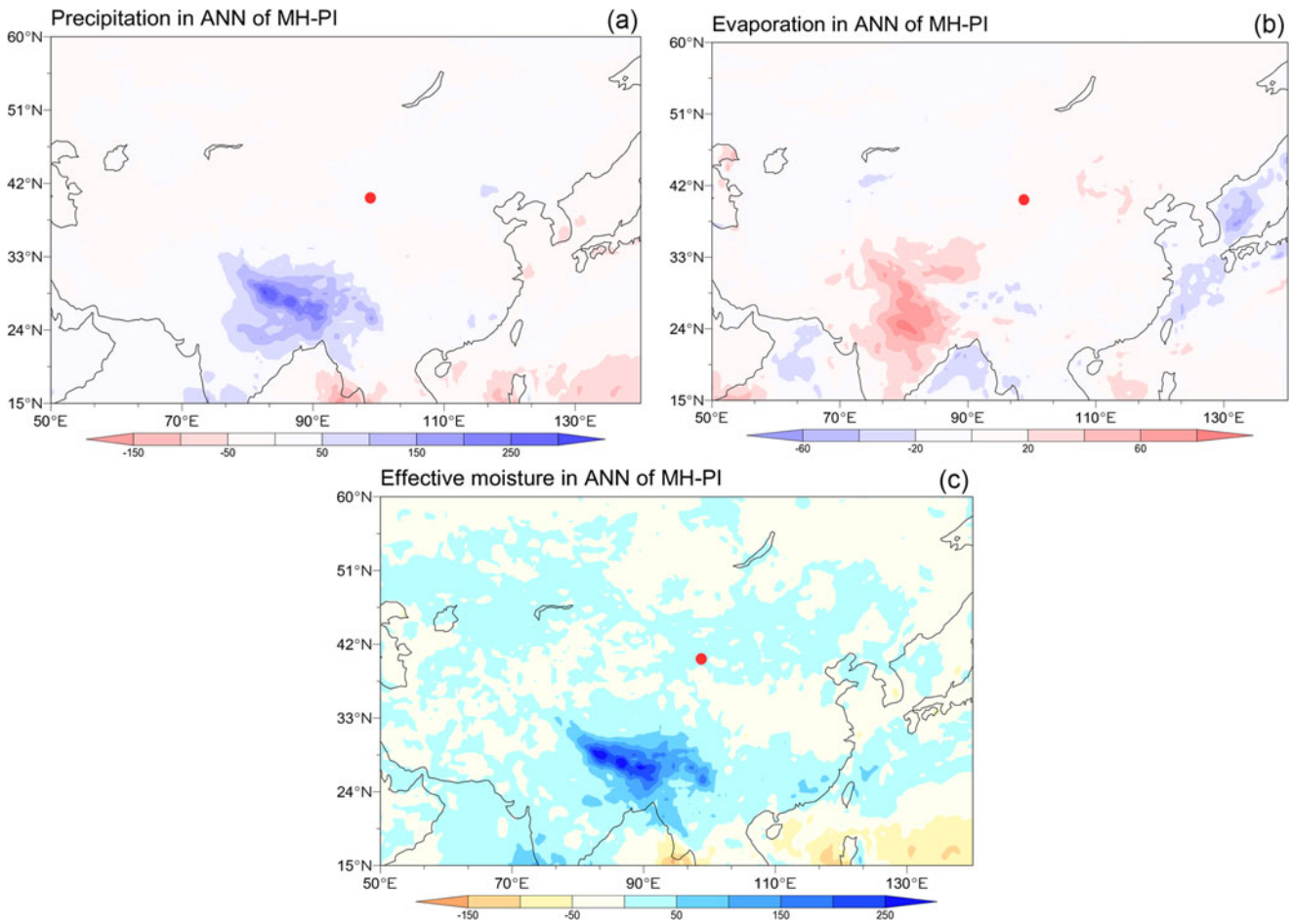

Figure 7. Multi-model ensemble results from PMIP3-CMIP5. (**a–c**) Difference of annual mean precipitation (mm/month), evaporation (mm/month), and effective moisture (mm/month) between the MH and PI, respectively. The red dot represents the BHZ section.

Zhang et al., 2016). Consequently, we suggest that the slight wetting trend in the BHZ section since the late LH results from the intensification of westerlies and the weakening of the Asian winter monsoon.

High-resolution and precisely dated speleothem and lake records from south and north China, the typical East Asian summer monsoon region, indicated that a strong summer monsoon and a humid climate occurred during the Early and Middle Holocene, and a weakened summer monsoon and a drier climate prevailed during the Late Holocene (Xiao et al., 2006; Cosford et al., 2008; Chen et al., 2015) (Fig. 9c–e). In the area influenced by the westerlies, most of the paleoclimate records documented a dry EH to a wetter MH and a moderately humid LH (Fig. 9f–h) (Chen et al., 2008, 2016b; Liu et al., 2008; Wolff et al., 2017), which is out of phase with records in AM regions. Hence, regional climate evolution and hydrological conditions on millennial timescales could differentiate between the effects of the AM and the westerlies. Figure 9 illustrates the similarity between the Asian summer monsoon pattern (Fig. 9c–e) and our records (Fig. 9a, b), which all indicate that the Asian summer monsoon induced by summer insolation controlled MH climate changes (Liu et al., 2007). Additionally, the westerlies-controlled proxy records (Fig. 9f–h) indicate that precipitation has increased gradually since the LH and generally is correlated with the slight wetting trend in the BHZ section.

Comparison of paleoclimate records between the BHZ section and other sites in the adjacent region

The Holocene climate evolution history in the Hexi Corridor and its surroundings has been widely reported and many high-resolution records from adjacent areas have been presented. Multivariate statistics from the terminal lake of Heihe River–the eastern Juyan paleolake indicate a climate optimum at 5400–4000 cal yr BP (Herzschuh et al., 2004; Hartmann and Wünnemann, 2009), which is essentially coincident with our results of the late MH humid climate (ca. 4400 to ca. 3500 cal yr BP). The interpretation of climate history in the Badain Jaran Desert suggested that the wet MH climate prevailed in the entire Badain Jaran Desert (Yang et al., 2011). In addition, the humid climate period (ca. 4400 to ca. 3500 cal yr BP) in the BHZ section is coincident with the 4.2 ka events. Holocene climatic records of the East Asian summer monsoon indicated that the 4.2 ka event was characterized by cold, dry conditions in China with less monsoonal moisture reaching northern China (Wang et al., 2005; Tan et al., 2018). The climatic conditions in the BHZ section during the time were, however, different from previous views. In fact, we argue that the relatively low resolution compared to the stalagmite records means that climate reconstruction in the BHZ section is not suitable for accurately indicating 4.2 ka events. The synthesis of evidence from lake sediments in arid Central Asia

https://doi.org/10.1017/qua.2023.37 Published online by Cambridge University Press

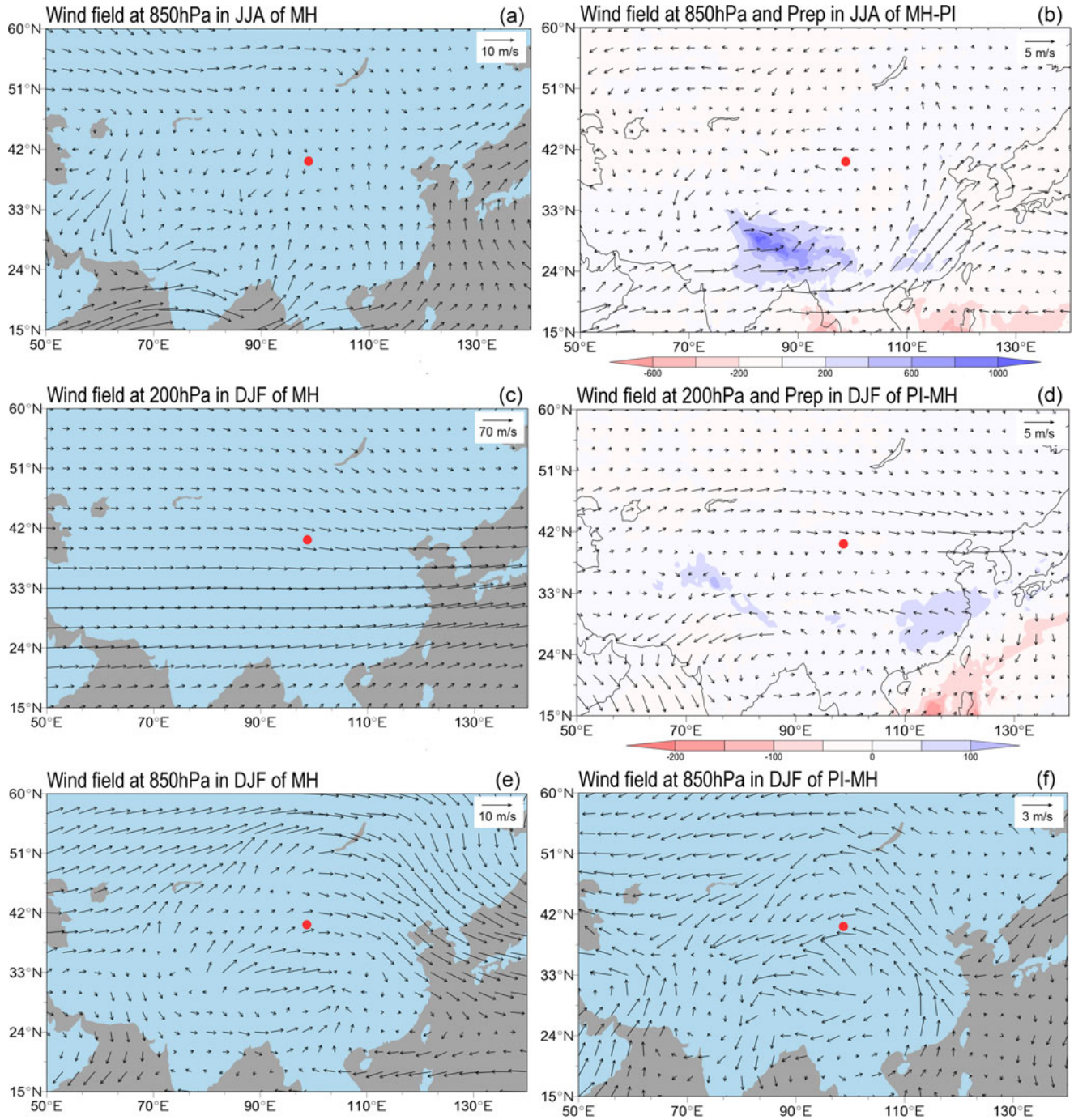

Figure 8. Multi-model ensemble results from PMIP3-CMIP5. Averaged wind field (m/s) at 850 hPa (**a, e**) and 200 hPa (**c**) isobaric in summer and winter during the MH, and the differential wind field at 850 hPa (**b, f**) and 200 hPa (**d**) isobaric in summer and winter between the MH and PI. Prep represents the precipitation, and the scale and shade indicate the difference of precipitation (mm/month) between PI and MH. JJA = June–July–August; DJF = December–January–February.

indicates that the moisture evolution pattern is characterized by a moderately wet LH, providing a reference for the slight wetting trend in the late LH in the BHZ section (Chen et al., 2008). Collectively, although studies presented in this section brought up contradictory ideas about Holocene climate evolution, the humid climate in the MH and LH also is similar to the published records found in northern and western China (Zhou et al., 2001).

The difference in climate interpretation is a function of the complexity of Holocene climate change near the northwest margin of the Asian summer monsoon (Zhao et al., 2007). The results of palynological reconstruction from the Dunde ice core implied that the enhanced Asian summer monsoon may have extended northward beyond the current northernmost edge to the Dunde ice core and the westernmost part of the Tibetan Plateau, leading to the high palynological concentration in the Holocene (Liu et al, 1998). The comprehensive analysis of carbonate oxygen isotope records suggested a significant influence of the winter monsoon and westerlies on climate and environmental change in Sugan Lake over the past 2700 years (Zhou, 2007).

https://doi.org/10.1017/qua.2023.37 Published online by Cambridge University Press

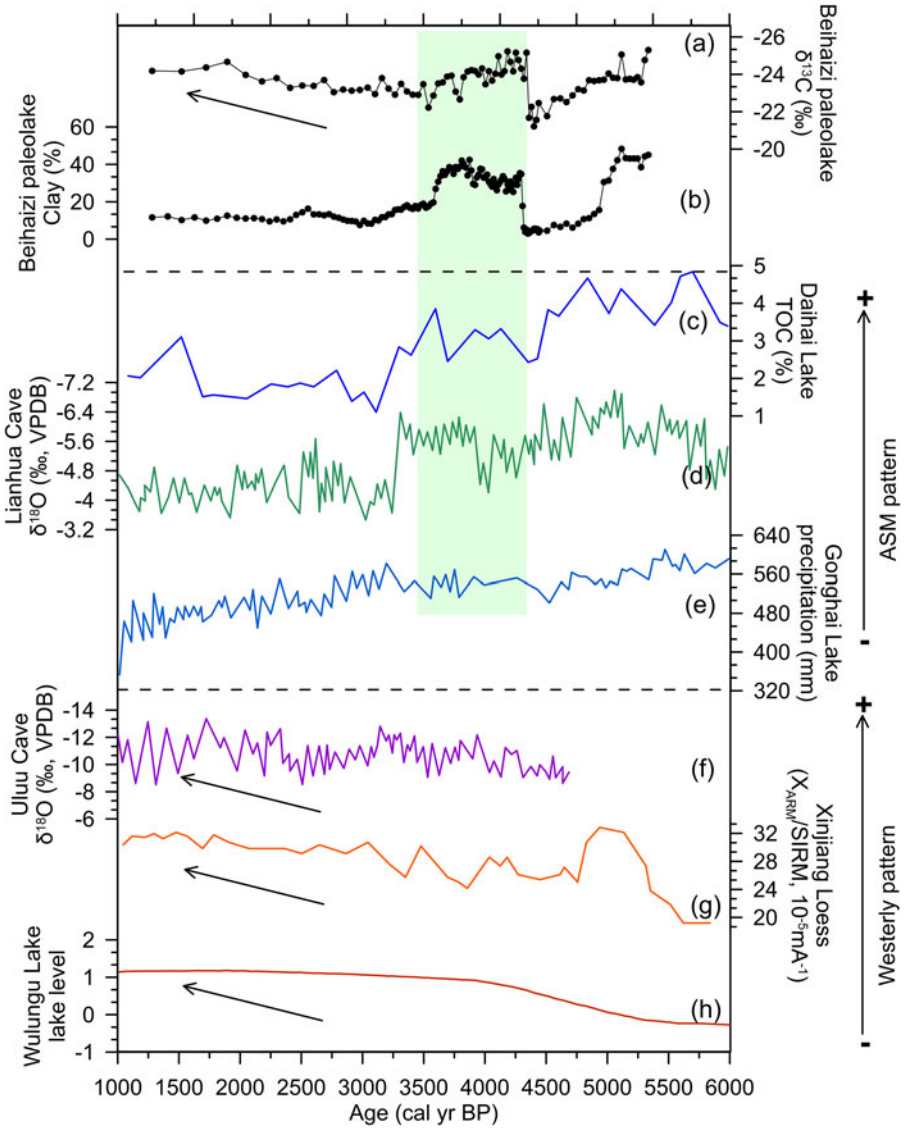

Figure 9. Intersite comparisons of regional paleoclimate records. (**a, b**) $\delta^{13}C_{org}$ and clay content, respectively, in the BHZ section of the Beihaizi paleolake in this study; (**c**) TOC content in Daihai Lake (Xiao et al., 2006); (**d**) stalagmite $\delta^{18}O$ in Lianhua Cave, eastern China (Cosford et al., 2008); (**e**) pollen-based quantitative precipitation reconstruction from Gonghai Lake, northern China (Chen et al., 2015); (**f**) stalagmite $\delta^{18}O$ in Uluu Cave, Central Asia (Wolff et al., 2017); (**g**) χ_{ARM}/SIRM ratio in the Xinjiang Loess (Chen et al., 2016b); (**h**) lake level change of Wulungu Lake (Liu et al., 2008). ARM = anhysteretic remanent magnetization; SIRM = saturation isothermal remanent magnetization.

Considering the factors and mechanisms controlling the humid climate in the MH in the eastern Juyan paleolake, several studies assumed that the interplay of the East Asian summer monsoon and the westerly waves resulted in increased runoff, refilling of the aquifer, and the increase of lake-internal organic carbon production in a lacustrine environment (An et al., 2000; Wünnemann et al., 2007; Hartmann and Wünnemann, 2009). Previous studies in the Badain Jaran Desert have proposed that the periodic change of westerlies and the AM was an essential factor in controlling the humid period (Yang et al., 2003). Further investigation concluded that the strengthened East Asian summer monsoon triggered wetter climate in the Badain Jaran Desert in the Holocene, which was linked with increasing insolation (Yang et al., 2010). The climate simulations of Feng and Yang (2019) demonstrated that the Asian summer monsoon brought abundant moisture to the Alashan Sand seas and the eastern Beihaizi paleolake in the period 8.2–4.2 ka BP, which caused high precipitation and the humid climate. Moreover, the Holocene climate change revealed by elemental geochemical records of Tiaohu Lake in the northwestern Jinta Basin may be jointly affected by the AM and westerlies (X. Li et al., 2013). Reconstructed effective moisture changes in Huahai Lake near the BHZ section were influenced by the AM, westerlies, and evaporation (Wang et al., 2013). The significant retreat of lake level and the lower deposition rate in Yanchi Lake since the MH indicated the monsoon effects on the northwest margin of the Asian summer monsoon (Y. Li et al., 2013). The Holocene paleoclimate records of Qinghai Lake show the evolution of climate and environment controlled by the Asian summer monsoon (Lister et al., 1991; Shen et al., 2005; Liu et al., 2007). On account of the complex climate of the northwestern margin of the summer monsoon, the pollen results of Hurleg Lake indicate that the Holocene humidity variability in the northeastern QTP was mainly controlled by westerlies and regional topography (Fan et al., 2014). Analysis of Hala Lake sedimentary cores found that the fluctuation of water levels in the Middle to Late Holocene was mainly controlled by westerly water vapor (Yan and Wünnemann, 2014).

In summary, the interaction between the westerlies and AM has a vital role in climate change in the middle part of the Hexi Corridor in the northern margin of the QTP. Our results demonstrate that strengthening Asian summer monsoon and increasing effective humidity dominated the late MH humid climate. On the

https://doi.org/10.1017/qua.2023.37 Published online by Cambridge University Press

other hand, the slight wetting trend since the late LH is mainly linked to enhanced westerlies and weakened Asian winter monsoon. Consequently, this study provides information for evaluating the interaction between the westerlies and AM and emphasizes the complex climate pattern under the control of diverse atmospheric systems in the northern margin of the QTP and the challenges for future predictions.

CONCLUSIONS

A new multiple-proxy dataset, including grain size, $\delta^{13}C_{org}$, $\delta^{18}O$, TOC, TN, C/N ratio, and MS, from the BHZ section taken in the Beihaizi paleolake was used to reconstruct climate change in the middle part of the Hexi Corridor in the northern margin of the QTP since 5334 cal yr BP. The analysis of all proxies indicated that high lake levels with humid climate occurred in the late MH (ca. 4400 to ca. 3500 cal yr BP). Despite the overall transition to an aeolian environment in the LH, there has been a slight wetting trend since the late LH.

Simulated precipitation, evaporation, and effective moisture based on the PMIP3-CMIP5 multi-model ensemble simulations verified the climate history and its possible causes in the MH and LH. In the MH, the Asian summer monsoon steadily strengthened, which favored high lake levels and humid climate. Increase of the surrounding vegetation since the late LH might result from enhanced westerlies, weakening Asian winter monsoon, and low evaporation. This climate pattern is different from those in the AM region or the westerlies-affected region and suggests a significant effect of the interaction between the AM and westerlies on Holocene climate change in the Hexi Corridor. The reconstruction and dynamic analysis of the lake and climate evolution presented in this study contribute to understanding their links with the AM and westerlies. Future work should focus on extending the AM and westerly records across multiple time scales in the northern QTP.

Supplementary Material. The supplementary material for this article can be found at https://doi.org/10.1017/qua.2023.37

Acknowledgments. This research was supported by the National Natural Science Foundation of China (Grant No. 42077415); the Second Tibetan Plateau Scientific Expedition and Research Program (STEP) (Grant No. 2019QZKK0202); the 111 Project (BP0618001). Data and software are available at https://doi.org/10.5281/zenodo.6407798.

REFERENCES

An, C., Feng, Z., Barton, L., 2006. Dry or humid? Mid-Holocene humidity changes in arid and semi-arid China. *Quaternary Science Reviews* **25**, 351–361.

An, C., Zhao, J., Tao, S., Lv, Y., Dong, W., Li, H., Jin, M., Wang, Z., 2011. Dust variation recorded by lacustrine sediments from arid Central Asia since ~15 cal ka BP and its implication for atmospheric circulation. *Quaternary Research* **75**, 566–573.

An, Z., Colman, S.M., Zhou, W., Li, X., Brown, E.T., Jull, A.T., Cai, Y., *et al.*, 2012. Interplay between the Westerlies and Asian monsoon recorded in Lake Qinghai sediments since 32 ka. *Scientific Reports* **2**, 619. https://doi.org/10.1038/srep00619.

An, Z., Porter, S.C., Kutzbach, J.E., Wu, X., Wang, S., Liu, X., Li, X., Zhou, W., 2000. Asynchronous Holocene optimum of the East Asian monsoon. *Quaternary Science Reviews* **19**, 743–762.

Aravena, R., Warner, B.G., MacDonald, G.M., Hanf, K.I., 1992. Carbon isotope composition of lake sediments in relation to lake productivity and radiocarbon dating. *Quaternary Research* **37**, 333–345.

Berger, A., Loutre, M.F., 1991. Isolation values for the climate of the last 10 million years. *Quaternary Science Reviews* **10**, 297–317.

Berner, R.A., 1981. A new geochemical classification of sedimentary environments. *Journal of Sedimentary Research* **51**, 359–369.

Bowen, R., 1991. *Isotopes and Climates*. Elsevier Applied Science, London.

Briegleb, B.P., Bitz, C.M., Hunke, E.C., Lioscomb, W.H., Holland, M.M., Schramm, J.L., Moritz, A.R., 2004. Scientific description of the sea ice component in the community climate system model, version 3. *NCAR Technical Report* **463**. University Corporation for Atmospheric Research. http://dx.doi.org/10.5065/D6HH6H1P.

Bronk Ramsey, C., 2009. Bayesian analysis of radiocarbon dates. *Radiocarbon* **51**, 337–360.

Bronk Ramsey, C., Lee, S., 2013. Recent and planned developments of the program OxCal. *Radiocarbon* **55**, 720–730.

Chen, F., Chen, J., Holmes, J., Boomer, I., Austin, P., Gates, J.B., Wang, N., Brooks, S., Zhang, J., 2010. Moisture changes over the last millennium in arid central Asia: a review, synthesis and comparison with monsoon region. *Quaternary Science Reviews* **29**, 1055–1068.

Chen, F., Chen, J., Huang, W., Chen, S., Huang, X., Jin, L., Jia, J., *et al.*, 2019. Westerlies Asia and monsoonal Asia: spatiotemporal differences in climate change and possible mechanisms on decadal to sub-orbital timescales. *Earth-Science Reviews* **192**, 337–354.

Chen, F., Jia, J., Chen, J., Li, G., Zhang, X., Xie, H., Xia, D., Huang, W., An, C., 2016b. A persistent Holocene wetting trend in arid central Asia, with wettest conditions in the late Holocene, revealed by multi-proxy analyses of loess-paleosol sequences in Xinjiang, China. *Quaternary Science Reviews* **146**, 134–146

Chen, F., Wu, D., Chen, J., Zhou, A., Yu, J., Shen, J., Wang, S., Huang, X., 2016a. Holocene moisture and East Asian summer monsoon evolution in the northeastern Tibetan Plateau recorded by Lake Qinghai and its environs: a review of conflicting proxies. *Quaternary Science Reviews* **154**, 111–129.

Chen, F., Xu, Q., Chen, J., Birks, H.J.B., Liu, J., Zhang, S., Jin, L., *et al.*, 2015. East Asian summer monsoon precipitation variability since the last deglaciation. *Scientific Reports* **5**, 11186. https://doi.org/10.1038/srep11186.

Chen, F., Yu, Z., Yang, M., Ito, E., Wang, S., Madsen, D.B., Huang, X., *et al.*, 2008. Holocene moisture evolution in arid central Asia and its out-of-phase relationship with Asian monsoon history. *Quaternary Science Reviews* **27**, 351–364.

Chen, J., An, Z.S., Head, J., 1999. Variation of Rb/Sr ratio in the loess-paleosol sequences of Central China during the last 130,000 years and their implications for monsoon paleoclimatology. *Quaternary Research* **51**, 215–219.

Cheng, B., Chen, F., Zhang, J., 2013. Palaeovegetational and palaeoenvironmental changes since the last deglacial in Gonghe Basin, northeast Tibetan Plateau. *Journal of Geographical Sciences* **23**, 136–146.

Chiang, J.C., Fung, I.Y., Wu, C. H., Cai, Y.J., Edman, J.P., Liu, Y.M., 2015. Role of seasonal transitions and westerly jets in East Asian paleoclimate. *Quaternary Science Reviews* **108**, 111–129.

Cosford, J., Qing, H., Eglington, B., Mattey, D., Yuan, D., Zhang, M., Cheng, H., 2008. East Asian monsoon variability since the mid-Holocene recorded in a high-resolution, absolute-dated aragonite speleothem from eastern China. *Earth and Planetary Science Letters* **275**, 296–307.

Dodson, J., Li, X., Ji, M., Zhao, K., Zhou, X., Levchenko, V., 2009. Early bronze in two Holocene archaeological sites in Gansu, NW China. *Quaternary Research* **72**, 309–314.

Dufresne, J.-L., Foujols, M.-A., Denvil, S., Caubel, A., Marti, O., Aumont, O., Balkanski, Y., *et al.*, 2013. Climate change projections using the IPSL-CM_5 Earth System Model: from $CMIP_3$ to $CMIP_5$. *Climate Dynamics* **40**, 2123–2165.

Fan, Q., Ma, H., Wei, H., An, F., 2014. Holocene lake-level changes of Hurleg Lake on northeastern Qinghai-Tibetan Plateau and possible forcing mechanism. *The Holocene* **24**, 274–283.

Farquhar, G.D., Ehleringer, J.R., Hubrick, K.T., 1989. Carbon isotopic discrimination and photosynthesis. *Annual Review of Plant Physiology and Plant Molecular Biology* **40**, 503–537.

Feng, J., Sun, H., He, M., Gao, Z., Liu, J., Wu, X., An, Y., 2020. Quality assessments of shallow groundwaters for drinking and irrigation purposes: insights from a case study (Jinta basin, Heihe drainage area, northwest China). *Water* **12**, 2704. https://doi.org/10.3390/w12102704.

Feng, Y., Yang, X., 2019. Moisture sources of the Alashan Sand Seas in western Inner Mongolia, China during the Last Glacial Maximum and mid-Holocene. *Journal of Geographical Sciences* **29**, 2101–2121.

Gao, K., Jiang, X., He, Y., Hu, H. M., Shen, C. C., Zhang, X., 2023. Strong link between Asian summer monsoon and westerlies for the past 4750 years. *Palaeogeography, Palaeoclimatology, Palaeoecology* **609**, 111329. https://doi.org/10.1016/j.palaeo.2022.111329.

Gent, P.R., Danabasoglu, G., Donner, L.J., Holland, M.M., Hunke, E.C., Jayne, S.R., Lawrence, D.M., Neale, R.B., Rasch, P.J., Vertenstein, M., 2011. The community climate system model version 4. *Journal of Climate* **24**, 4973–4991.

Gou, X., Deng, Y., Gao, L., Chen, F., Cook, E., Yang, M., Zhang, F., 2015. Millennium tree-ring reconstruction of drought variability in the eastern Qilian Mountains, northwest China. *Climate Dynamics* **45**, 1761–1770.

Greig, A., David, H., 2015. New methods for unmixing sediment grain size data. *Geochemistry, Geophysics, Geosystems* **16**, 4494–4506.

Hartmann, K., Wünnemann, B., 2009. Hydrological changes and Holocene climate variations in NW China, inferred from lake sediments of Juyanze palaeolake by factor analyses. *Quaternary International* **194**, 28–44.

Herzschuh, U., Borkowski, J., Schewe, J., Mischke, S., Tian, F., 2014. Moisture advection feedback supports strong early-to-mid Holocene monsoon climate on the eastern Tibetan Plateau as inferred from a pollen-based reconstruction. *Palaeogeography, Palaeoclimatology, Palaeoecology* **402**, 44–54.

Herzschuh, U., Cao, X., Laepple, T., Dallmeyer, A., Telford, R.J., Ni, J., Chen, F., *et al.*, 2019. Position and orientation of the westerly jet determined Holocene rainfall patterns in China. *Nature Communications* **10**, 2376. https://doi.org/10.1038/s41467-019-09866-8.

Herzschuh, U., Tarasov, P., Wunnemann, B., Hartmann, K., 2004. Holocene vegetation and climate of the Alashan Plateau, NW China, reconstructed from pollen data. *Palaeogeography, Palaeoclimatology, Palaeoecology* **211**, 1–17.

Hofmann, J., Geyh, M.A., 1998. Untersuchungen zum ^{14}C-Reservoir Effekt an rezenten und fossilen lakustrinen Sedimenten aus dem Südosten der Badain Jaran Wüste (Innere Mongolei/VR China). *Berliner Geographische Abhandlungen* **63**, 83–98.

Horton, T.W., Defliese, W.F., Tripati, A.K., Oze, C., 2016. Evaporation induced ^{18}O and ^{13}C enrichment in lake systems: a global perspective on hydrologic balance effects. *Quaternary Science Reviews* **131**, 365–379.

Hu, J., Sha, Z., Ma, Y., Kong, F., Wang, Q., 2017. Characteristics of grain size and their environmental significance of sediment at the Buha estuary of Qinghai Lake. *Arid Zone Research* **34**, 445–451. [in Chinese]

Ji, Y., Xia, Z., 2007. Comparison and Primarily Interpretation of Magnetic Susceptibilities in Different Sediments. *Acta Geoscientica Sinica* **28**, 541–549. [in Chinese]

Jin, L., Chen, F., Morrill, C., Otto-Bliesner, B., Rosenbloom, N., 2012. Causes of Early Holocene desertification in arid central Asia. *Climate Dynamics* **38**, 1577–1591.

Kalnay, E., Kanamitsu, M., Kistler, R., Collins, W., Deaven, D., Gandin, L., Iredell, M., *et al.*, 1996. The NCEP/NCAR 40-year reanalysis project. *Bulletin of the American Meteorological Society* **77**, 437–472.

Kaufman, D., McKay, N., Routson, C., Erb, M., Dätwyler, C., Sommer, P., Heiri, O., Davis, B., 2020. Holocene global surface temperature: a multi-method reconstruction approach. *Scientific Data* **7**, 201. https://doi.org/10.1038/s41597-020-0530-7.

Kohn, M.J., 2010. Carbon isotope compositions of terrestrial C3 plants as indicators of (paleo) ecology and (paleo)climate. *Proceedings of the National Academy of Sciences* **107**, 19691–19695.

Kong, W., Swenson, L., Chiang, J., 2017. Seasonal transitions and the westerly jet in the Holocene East Asian summer monsoon. *Journal of Climate* **108**, 11–129.

Kranck, K., Smith, P.C., Milligan, T.G., 1996. Grain-size characteristics of fine-grained unflocculated sediments I: 'one-round' distributions. *Sedimentology* **43**, 589–594.

Lan, J., Wang, T., Dong, J., Kang, S., Cheng, P., Zhou, K., Liu, X., Wang, Y., Ma, L., 2021. The influence of ice sheet and solar insolation on Holocene moisture evolution in northern Central Asia. *Earth-Science Reviews* **217**, 103645. https://doi.org/10.1016/j.earscirev.2021.103645.

Lan, J., Xu, H., Liu, B., Sheng, E., Zhao, J., Yu, K., 2013. Paleoclimate implications of carbonate, organic matter, and their stable isotopes in lacustrine sediments: a review. *Chinese Journal of Ecology* **32**, 1326–1334. [in Chinese]

Li, B., 1998. An investigation and study on the desertification of the ancient oases from Han to Tang dynasties in the Heixi Corridor. *Acta Geographica Sinica* **53**, 106–115. [in Chinese]

Li, G., Wang, X., Zhang, X., Yan, Z., Liu, Y., Yang, H., Wang, Y., *et al.*, 2022. Westerlies-Monsoon interaction drives out-of-phase precipitation and asynchronous lake level changes between Central and East Asia over the last millennium. *Catena* **218**, 106568. https://doi.org/10.1016/j.catena.2022.106568.

Li, L., Lin, P., Yu, Y., Wang, B., Zhou, T., Liu, L., Liu, J., *et al.*, 2013. The flexible global ocean-atmosphere-land system model, Grid-point version 2: FGOALS-g2. *Advances in Atmospheric Sciences* **30**, 543–560.

Li, X., Ji, M., Dodson, J., Zhou, X., Zhao, K., Sun, N., Yang, Q., 2010. Records of element geochemistry on the bronze smelting in Hexi Corridor since 4200 aBP. *Journal of Lake Sciences* **22**, 103–109. [in Chinese]

Li, X., Liu. H., Zhao, K., Ji, M., Zhou, X., 2013. Holocene climate and environmental changes reconstructed from elemental geochemistry in the western Hexi Corridor. *Acta Anthropologica Sinica* **32**, 110–120. [in Chinese]

Li, X., Sun, N., Dodson, J., Ji, M., Zhao, K., Zhou, X., 2011. The impact of early smelting on the environment of Huoshiliang in Hexi Corridor, NW China, as recorded by fossil charcoal and chemical elements. *Palaeogeography, Palaeoclimatology, Palaeoecology* **305**, 329–336.

Li, Y., Han, L., Liu, X., Song, Y., Wang, Y., 2021. Correlation and anti-correlation of the Asian summer monsoon and westerlies during the Holocene. *Gondwana Research* **91**, 112–120.

Li, Y., Peng, S., Hao, L., Zhou, X., Li, H., 2022. Interactions of the westerlies and Asian summer monsoon since the last deglaciation in the northeastern Qinghai-Tibet Plateau. *Paleoceanography and Paleoclimatology* **37**, e2022PA004548. https://doi.org/10.1029/2022PA004548.

Li, Y., Peng, S., Liu, H., Zhang, X., Ye, W., Han, Q., Zhang, Y., Xu, L., Li, Y.C., 2020. Westerly jet stream controlled climate change mode since the Last Glacial Maximum in the northern Qinghai-Tibet Plateau. *Earth and Planetary Science Letters* **549**, 116529. https://doi.org/10.1016/j.epsl.2020.116529.

Li, Y., Wang, N., Chen, H., Li, Z., Zhou, X., Zhang, C., 2012. Tracking millennial-scale climate change by analysis of the modern summer precipitation in the marginal regions of the Asian monsoon. *Journal of Asian Earth Sciences* **58**, 78–87.

Li, Y., Wang, N., Li, Z., Cheng, H., 2011. The relationship among organic geochemical proxies and their palaeoenvironmental significances in the Zhuye Lake sediments. *Journal of Glaciology and Geocryology* **33**, 334–341. [in Chinese]

Li, Y., Wang, N., Li, Z., Zhou, X., Zhang, C., 2013. Climatic and environmental change in Yanchi Lake northwest China since the Late Glacial: a comprehensive analysis of lake sediments. *Journal of Geographical Sciences* **23**, 932–946.

Lister, G.S., Kelts, K., Zao, C., Yu, J., Niessen, F., 1991. Lake Qinghai, China: closed-basin lake levels and the oxygen isotope record for Ostracoda since the latest Pleistocene. *Palaeogeography, Palaeoclimatology, Palaeoecology* **84**, 141–162.

Liu, C., Zhang, J., Jiao, P., Mischke, S., 2016. The Holocene history of Lop Nur and its palaeoclimate implications. *Quaternary Science Reviews* **148**, 163–175.

Liu, K., Yao, Z., Thompson, L.G., 1998. A pollen record of Holocene climatic changes from the Dunde ice cap, Qinghai-Tibetan Plateau. *Geology* **26**, 135–138.

Liu, W., Li, X., An, Z., Xu, L., Zhang, Q., 2013. Total organic carbon isotopes: a novel proxy of lake level from Lake Qinghai in the Qinghai-Tibet Plateau, China. *Chemical Geology* **347**, 153–160.

Liu, X., Dong, H., Yang, X., Herzschuh, U., Zhang, E., Stuut, J.-B.W., Wang, Y., 2009. Late Holocene forcing of the Asian winter and summer monsoon as evidenced by proxy records from the northern Qinghai-Tibetan Plateau. *Earth and Planetary Science Letters* **280**, 276–284.

Liu, X., Herzschuh, U., Shen, J., Jiang, Q., Xiao, X., 2008. Holocene environmental and climatic changes inferred from Wulungu Lake in northern Xinjiang, China. *Quaternary Research* **70**, 412–425.

https://doi.org/10.1017/qua.2023.37 Published online by Cambridge University Press

Liu, X., Lai, Z., Yu, L., Sun, Y., Madsen, D., 2012. Luminescence chronology of aeolian deposits from the Qinghai Lake area in the northeastern Qinghai-Tibetan Plateau and its palaeoenvironmental implications. *Quaternary Geochronology* **10**, 37–43.

Liu, X., Shen, J., Wang, S., Wang, Y., Liu, W., 2007. Southwest monsoon changes indicated by oxygen isotope of ostracode shells from sediments in Lake Qinghai since the late Glacial. *Chinese Science Bulletin* **52**, 539–544.

Liu, X., Vandenberghe, J., An, Z., Li, Y., Jin, Z., Dong, J., Sun, Y., 2016. Grain size of Lake Qinghai sediments: implications for riverine input and Holocene monsoon variability. *Palaeogeography, Palaeoclimatology, Palaeoecology* **449**, 41–51.

Long, H., Lai, Z., Wang, N., Zhang, J., 2011. A combined luminescence and radiocarbon dating study of Holocene lacustrine sediments from arid northern China. *Quaternary Geochronology* **6**, 1–9.

Lu, H., Zhao, C., Mason, J., Yi, S., Zhao, H., Zhou, Y., Ji, J., Swinehart, J., Wang, C., 2011. Holocene climatic changes revealed by aeolian deposits from the Qinghai Lake area (northeastern Qinghai-Tibetan Plateau) and possible forcing mechanisms. *The Holocene* **21**, 297–304.

Meyer, I., Davies, G.R., Vogt, C., Kuhlmann, H., Stuut, J.-B.W., 2013. Changing rainfall patterns in NW Africa since the Younger Dryas. *Aeolian Research* **10**, 111–123.

Meyers, P.A., Lallier-Vergès, E., 1999. Lacustrine sedimentary organic matter records of late Quaternary paleoclimates. *Journal of Paleolimnology* **21**, 345–372.

Nagashima, K., Tada, R., Matsui, H., Irino, T., Tani, A., Toyoda, S., 2007. Orbital- and millennial-scale variations in Asian dust transport path to the Japan Sea. *Palaeogeography, Palaeoclimatology, Palaeoecology* **247**, 144–161.

Nagashima, K., Tada, R., Tani, A., Sun, Y., Isozaki, Y., Toyoda, S., Hasegawa, H., 2011. Millennial-scale oscillations of the westerly jet path during the last glacial period. *Journal of Asian Earth Sciences* **40**, 1214–1220.

Nagashima, K., Tada, R., Toyoda, S., 2013. Westerly jet-East Asian summer monsoon connection during the Holocene. *Geochemistry, Geophysics, Geosystems* **14**, 5041–5053.

Peng, S., Li, Y., Liu, H., Han, Q., Zhang, X., Feng, Z., Chen, D., Ye, W., Zhang, Y., 2022. Formation and evolution of mountainous aeolian sediments in the northern Tibet Plateau and their links to the Asian winter monsoon and westerlies since the last glacial maximum. *Progress in Physical Geography: Earth and Environment* **46**, 43–60.

Peng, Y.J., Xiao, J.L., Nakamura, T., Liu, B.L., Inouchi, Y., 2005. Holocene East Asian monsoonal precipitation pattern revealed by grain-size distribution of core sediments of Daihai Lake in inner Mongolia of north-central China. *Earth and Planetary Science Letters* **233**, 467–479.

Prins, M.A., Bouwer, L.M., Beets, C.J., Troelstra, S.R., Weltje, G.J., Kruk, R.W., Kuijpers, A., Vroon, P.Z., 2002. Ocean circulation and iceberg discharge in the glacial North Atlantic: inferences from unmixing of sediment size distributions. *Geology* **30**, 555–558.

Qiang, M., Chen, F., Zhang, J., Gao, S., Zhou, A., 2005. Climate change recorded by stable isotope of carbonate sediments in Sugan Lake since 2 kaBP. *Chinese Science Bulletin* **50**, 1930–1939. [in Chinese with English abstract]

Qiang, M., Song, L., Chen, F., Li, M., Liu, X., Wang, Q., 2013. A 16-ka lake-level record inferred from macrofossils in a sediment core from Genggahai Lake, northeastern Qinghai-Tibetan Plateau (China). *Journal of Paleolimnology* **49**, 575–590.

Qiang, M., Song, L., Jin, Y., Li, Y., Liu, L., Zhang, J., Zhao, Y., Chen, F., 2017. A 16-ka oxygen-isotope record from Genggahai Lake on the northeastern Qinghai-Tibetan Plateau: hydroclimatic evolution and changes in atmospheric circulation. *Quaternary Science Reviews* **162**, 72–87.

Raddatz, T.J., Reick, C.H., Knorr, W., Kattge, J., Roeckner, E., Schnur, R., Schnitzler, K.G., Wetzel, P., Jungclaus, J., 2007. Will the tropical land biosphere dominate the climate–carbon cycle feedback during the twenty-first century? *Climate Dynamics* **29**, 565–574.

Randall, D.A., Wood, R.A., Bony, S., Colman, R., Taylor, K.E., 2007. Climate models and their evaluation. In: Solomon, S., Qin, D., Manning, M., Chen, Z., Marquis, M., Averyt, K.B., Tignor, M., Miller, H.L. (Eds.), *Climate Change 2007: The Physical Science Basis. Contribution of Working Group I to the Fourth Assessment Report of the Intergovernmental Panel on Climate Change*. Cambridge University Press, Cambridge, UK, New York, pp. 589–662.

Rao, Z., Chen, F., Zhang, X., Xu, Y., Xue, Q., Zhang, P., 2012. Spatial and temporal variations of C_3/C_4 relative abundance in global terrestrial ecosystem since the Last Glacial and its possible driving mechanisms. *Chinese Science Bulletin* **57**, 4024–4035.

Rao, Z., Guo, W., Cao, J., Shi, F., Jiang, H., Li, C., 2017. Relationship between the stable carbon isotopic composition of modern plants and surface soils and climate: a global review. *Earth-Science Reviews* **165**, 110–119.

Reimer, P.J., Austin, W.E.N., Bard, E., Bayliss, A., Blackwell, P.G., Bronk Ramsey, C., Butzin, M., *et al.*, 2020. The IntCal20 Northern Hemisphere radiocarbon age calibration curve (0–55 cal kBP). *Radiocarbon* **62**, 725–757.

Rotstayn, L., Collier, M., Dix, M., Feng, Y., Gordon, H., O'Farrell, S., Smith, I., Syktus, J., 2010. Improved simulation of Australian climate and ENSO-related climate variability in a GCM with an interactive aerosol treatment. *International Journal of Climatology* **30**, 1067–1088.

Sampe, T., Xie, S.-P., 2010. Large-scale dynamics of the Meiyu-Baiu rainband: environmental forcing by the Westerly Jet. *Journal of Climate* **23**, 113–134.

Schmidt, G.A., Kelley, M., Nazarenko, L., Ruedy, R., Russell, G.L., Aleinov, I., Bauer, M., *et al.*, 2014. Configuration and assessment of the GISS ModelE2 contributions to the CMIP5 archive. *Journal of Advances in Modeling Earth Systems* **6**, 141–184.

Shen, J., Liu, X., Wang, S., Matsumoto, R., 2005. Palaeoclimatic changes in the Qinghai Lake area during the last 18,000 years. *Quaternary International* **136**, 131–140.

Sun, Q., Wang, S., Zhou, J., Shen, J., Cheng, P., Xie, X., Wu, F., 2009. Lake surface fluctuations since the late glaciation at Lake Daihai, north central China: a direct indicator of hydrological process response to East Asian monsoon climate. *Quaternary International* **194**, 45–54.

Sun, Y., Clemens, S.C., Morrill, C., Lin, X., Wang, X., An, Z., 2012. Influence of Atlantic meridional overturning circulation on the East Asian winter monsoon. *Nature Geoscience* **5**, 46–49.

Sun, Y., Wang, X., Liu, Q., Clemens, S.C., 2010. Impacts of post-depositional processes on rapid monsoon signals recorded by the last glacial loess deposits of northern China. *Earth and Planetary Science Letters* **289**, 171–179.

Tan, L., Cai, Y., Cheng, H., Edwards, R.L., Gao, Y., Xu, H., Zhang, H., An, Z., 2018. Centennial- to decadal-scale monsoon precipitation variations in the upper Hanjiang River region, China over the past 6650 years. *Earth and Planetary Science Letters* **482**, 580–590.

Terry, J.P., Goff, J., 2014. Megaclasts: proposed revised nomenclature at the coarse end of the Udden-Wentworth grain-size scale for sedimentary particles. *Journal of Sedimentary Research* **84**, 192–197.

Thompson, L.G., Mosley-Thompson, E., Wu, X., Xie, Z., 1988. Wisconsin/Würm glacial stage ice in the subtropical Dunde ice cap, China. *GeoJournal* **17**, 517–523.

Voldoire, A., Sanchez-Gomez, E., Mélia, D.S.y, Decharme, B., Cassou, C., Sénési, S., Valcke, S., *et al.*, 2013. The CNRM-$CM_{5.1}$ global climate model: description and basic evaluation. *Climate Dynamics* **40**, 2091–2121.

Wang, B., Liu, J., Kim, H.J., Webster, P.J., Yim, S.Y., 2012. Recent change of the global monsoon precipitation (1979–2008). *Climate Dynamics* **39**, 1123–1135.

Wang, N., Li, Z., Li, Y., Cheng, H., 2013. Millennial-scale environmental changes in the Asian monsoon margin during the Holocene, implicated by the lake evolution of Huahai Lake in the Hexi Corridor of northwest China. *Quaternary International* 313–314, 100–109.

Wang, N., Li, Z., Li, Y., Zhu, J., 2011. The Chronology and characteristics of sediments since late glacial in Huahai Lake, Hexi Corridor, NW China. *Acta Sedimentologica Sinica* **29**, 552–560. [in Chinese]

Wang, P., Wang, B., Cheng, H., Fasullo, J., Guo, Z., Kiefer, T., Liu, Z., 2017. The global monsoon across time scales: mechanisms and outstanding issues. *Earth-Science Reviews* **174**, 84–121.

Wang, W., Feng, Z., 2013. Holocene moisture evolution across the Mongolian Plateau and its surrounding areas: a synthesis of climatic records. *Earth-Science Reviews* **122**, 38–57.

Wang, Y., Cheng, H., Edwards, R., An, Z., Wu, J., Shen, C., Dorale, J., 2001. A high-resolution absolute-dated late Pleistocene monsoon record from Hulu Cave, China. *Science* **294**, 2345–2348.

https://doi.org/10.1017/qua.2023.37 Published online by Cambridge University Press

Wang, Y., Cheng, H., Edwards, R.L., He, Y., Kong, X., An, Z., Wu, J., Kelly, M., Dykoski, C., 2005. The Holocene Asian monsoon: links to solar changes and North Atlantic climate. *Science* **308**, 854–857.

Wang, Y., Liu, X., Herzschuh, U., 2010. Asynchronous evolution of the Indian and East Asian Summer Monsoon indicated by Holocene moisture patterns in monsoonal central Asia. *Earth-Science Reviews* **103**, 135–153.

Watanabe, S., Hajima, T., Sudo, K., Nagashima, T., Takemura, T., Okajima, H., Nozawa, T., *et al.*, 2011. MIROC-ESM 2010: model description and basic results of CMIP5-20c3m experiments. *Geoscientific Model Development* **4**, 845–872.

Weltje, G.J., Prins, M.A., 2003. Muddled or mixed? Inferring palaeoclimate from size distributions of deep-sea clastics. *Sedimentary Geology* **162**, 39–62.

Wen, R., Xiao, J., Chang, Z., Zhai, D., Xu, Q., Li, Y., Itoh, S., Lomtatidze, Z., 2010. Holocene climate changes in the mid-high-latitude-monsoon margin reflected by the pollen record from Hulun Lake, northeastern Inner Mongolia. *Quaternary Research* **73**, 293–303.

Wolff, C., Plessen, B., Dudashvilli, A.S., Breitenbach, S.F., Cheng, H., Edwards, L.R., Strecker, M.R., 2017. Precipitation evolution of Central Asia during the last 5000 years. *The Holocene* **27**, 142–154.

Wu, D., Zhou, A.F., Chen, X.M., Yu, J.Q., Zhang, J.W., Sun, H.L., 2015. Hydrological and ecosystem response to abrupt changes in the Indian monsoon during the last glacial, as recorded by sediments from Xingyun Lake, Yunnan, China. *Palaeogeography, Palaeoclimatology, Palaeoecology* **421**, 15–23.

Wu, D., Zhou, A., Zhang, J., Chen, J., Li, G., Wang, Q., Chen, L., *et al.*, 2020. Temperature-induced dry climate in basins in the northeastern Tibetan Plateau during the Early to Middle Holocene. *Quaternary Science Reviews* **237**, 106311. https://doi.org/10.1016/j.quascirev.2020.106311.

Wu, R., 1993. Magnetic susceptibility and frequency dependent susceptibility of lake sediments and their paleoclimatic implication—the case of recent sediments of Qinghai Lake and Daihai Lake. *Journal of Lake Sciences* **5**, 128–135. [in Chinese]

Wünnemann, B., Hartmann, K., Janssen, M., Zhang, H.C., 2007. Responses of Chinese desert lakes to climate instability during the past 45,000 years. In: Madsen, D.B., Chen, F.H., Gao, X. (Eds.), *Late Quaternary Climate Change and Human Adaptation in Arid China*. Developments in Quaternary Science, vol. 9, Elsevier, Amsterdam, pp. 11–24.

Xiao, J., Fan, J., Zhou, L., Zhai, D., Wen, R., Qin, X., 2013. A model for linking grain size component to lake level status of a modern clastic lake. *Journal of Asian Earth Sciences* **69**, 149–158.

Xiao, J., Nakamura, T., Lu, H., Zhang, G., 2002. Holocene climate changes over the desert/loess transition of north-central China. *Earth and Planetary Science Letters* **197**, 11–18.

Xiao, J., Wu, J., Si, B., Liang, W., Nakamura, T., Liu, B., Inouchi, Y., 2006. Holocene climate changes in the monsoon/arid transition reflected by carbon concentration in Daihai Lake of Inner Mongolia. *The Holocene* **16**, 551–560.

Yan, D., Wünnemann, B., 2014. Late Quaternary water depth changes in Hala Lake, northeastern Tibetan Plateau, derived from ostracod assemblages and sediment properties in multiple sediment records. *Quaternary Science Reviews* **95**, 95–114.

Yang, B., Qin, C., Bräuning, A., Osborn, T.J., Trouet, V., Ljungqvist, F.C., Esper, J., *et al.*, 2021. Long-term decrease in Asian monsoon rainfall and abrupt climate change events over the past 6,700 years. *Proceedings of the National Academy of Sciences* **118**, e2102007118. https://doi.org/10.1073/pnas.2102007118.

Yang, X., Liu, T., Xiao, H., 2003. Evolution of megadunes and lakes in the Badain Jaran Desert, Inner Mongolia, China during the last 31000 yrs. *Quaternary International* **104**, 99–112.

Yang, X., Ma, N., Dong, J., Zhu, B., Xu, B., Ma, Z., Liu, J., 2010. Recharge to the inter-dune lakes and Holocene climatic changes in the Badain Jaran Desert, western China. *Quaternary Research* **73**, 10–19.

Yang, X., Scuderi, L., Paillou, P., Liu, Z., Li, H., Ren, X., 2011. Quaternary environmental changes in the drylands of China—a critical review. *Quaternary Science Reviews* **30**, 3219–3233.

Yao, T.D., G.Thompson, [sic] L., 1992. Dunde ice core record and past 5 ka temperature change. *Science in China Series B-Chemistry, Life Sciences & Earth Sciences* **22**, 1089–1093. https://doi.org/10.1360/zb1992-22-10-1089. [in Chinese]

Yu, S., Ricketts, R.D., Colman, S.M., 2009. Determining the spatial and temporal patterns of climate changes in China western interior during the last 15 ka from lacustrine oxygen isotope records. *Journal of Quaternary Science* **24**, 237–247.

Yuan, D., Cheng, H., Edwards, R.L., Dykoski, C.A., Kelly, M.J., Zhang, M., Qing, J., *et al.*, 2004. Timing, duration, and transitions of the last interglacial Asian monsoon. *Science* **304**, 575–578.

Yukimoto, S., Adachi, Y., Hosaka, M., Sakami, T., Yoshimura, H., Hirabara, M., Tanaka, T.Y., Shindo, E., Tsujino, H., Deushi, M., 2012. A new global climate model of the Meteorological Research Institute—MRI-CGCM3—model description and basic performance. *Journal of the Meteorological Society of Japan* 90A, 23–64.

Zhang, H., Ming, Q., Lei, G., Zhang, W., Fan, H., Chang, F., Wünnemann, B., Hartmann, K., 2006. Dilemma of dating on lacustrine deposits in an hyperarid inland basin of NW China. *Radiocarbon* **48**, 219–226.

Zhang, J., Alexander, M.R., Gou, X., Deslauriers, A., Fonti, P., Zhang, F., Pederson, N., 2020. Extended xylogenesis and stem biomass production in *Juniperus przewalskii* Kom. during extreme late-season climatic events. *Annals of Forest Science* **77**, 99. https://doi.org/10.1007/s13595-020-01008-1.

Zhang, Q., Zhang, Y., Zhao, Y., Ma, J., 2011. Geochemical evolution of groundwater and hydrogeochemical modeling in Jinta Basin. *Arid Land Geography* **34**, 772–778.

Zhang, X., Jin, L., Huang, W., Chen, F., 2016. Forcing mechanisms of orbital-scale changes in winter rainfall over northwestern China during the Holocene. *The Holocene* **26**, 549–555.

Zhang, X., Jin, L., Lu, H., Park, W., Schneider, B., Latif, M., 2018. East-west contrast of northeast Asian summer precipitation during the Holocene. *Global and Planetary Change* **170**, 190–200.

Zhang, X., Liu, B., Chen, S., Fu, Z., Xie, T., Chen, F., 2022. Increased water vapor supply in winter and spring leading to the arid Central Asian wetting in last 6000 years. *Science China Earth Sciences* **65**, 1353–1367.

Zhang, Z., We, R., Wang, S., 1998. Implication of magnetic frequency dependent susceptibility on environmental variation from lacustrine sediment in Daihai Lake. *Geographical Research* **17**, 297–302. [in Chinese]

Zhao, C., Yu, Z., Zhao, Y., Ito, E., Kodama, K. P., Chen, F., 2010. Holocene millennial-scale climate variations documented by multiple lake-level proxies in sediment cores from Hurleg Lake, northwest China. *Journal of Paleolimnology* **44**, 995–1008.

Zhao, Q., Wang, N., Li, X., Cheng, H., Li. Y., Li, G., 2005. Environmental change around the Qingtu Lake since 9500 a BP. *Journal of Glaciology and Geocryology* **27**, 352–359.

Zhao, Y., Wu, F., Fang, X., Yang, Y., 2017. Altitudinal variations in the bulk organic carbon isotopic composition of topsoil in the Qilian Mountains area, NE Tibetan Plateau, and its environmental significance. *Quaternary International* **454**, 45–55.

Zhao, Y., Yu, Z., Chen, F., Ito, E., Zhao, C., 2007. Holocene vegetation and climate history at Hurleg Lake in the Qaidam Basin, northwest China. *Review of Palaeobotany and Palynology* **145**, 275–288.

Zheng, S., Shangguan, Z., 2007. Spatial patterns of foliar stable carbon isotope compositions of C_3 plant species in the Loess Plateau of China. *Ecological Research* **22**, 342–353.

Zhong, W., Xue, J.B., Cao, J., Zheng, Y., Ma, Q., Jun, O., Cai, Y., Zeng, Z., Liu, W., 2010. Bulk organic carbon isotope record of lacustrine sediments in Dahu Swamp, eastern Nanling Mountains in South China: implication for catchment environmental and climatic changes in the last 16000 years. *Journal of Asian Earth Sciences* **38**, 162–169.

Zhou, A., 2007. *Varve Chronology and Late Holocene Environmental Changes in Sugan Lake, Northern Qaidam Basin*. PhD thesis, Lanzhou University, Lanzhou, Gansu, China.

Zhou, W., Head, J., Deng, L., 2001. Climatic changes in northern China since the late Pleistocene and its response to global change. *Quaternary International* 83–85, 285–292.

Zhou, X., Li, Y., Zhang, C., Wang, Y., 2013. The response of organic geochemical proxies in Holocene lake sediments to millennial-scale climate change. *Journal of Salt Lake Research* **2013** (4), 1–9. [in Chinese]

https://doi.org/10.1017/qua.2023.37 Published online by Cambridge University Press